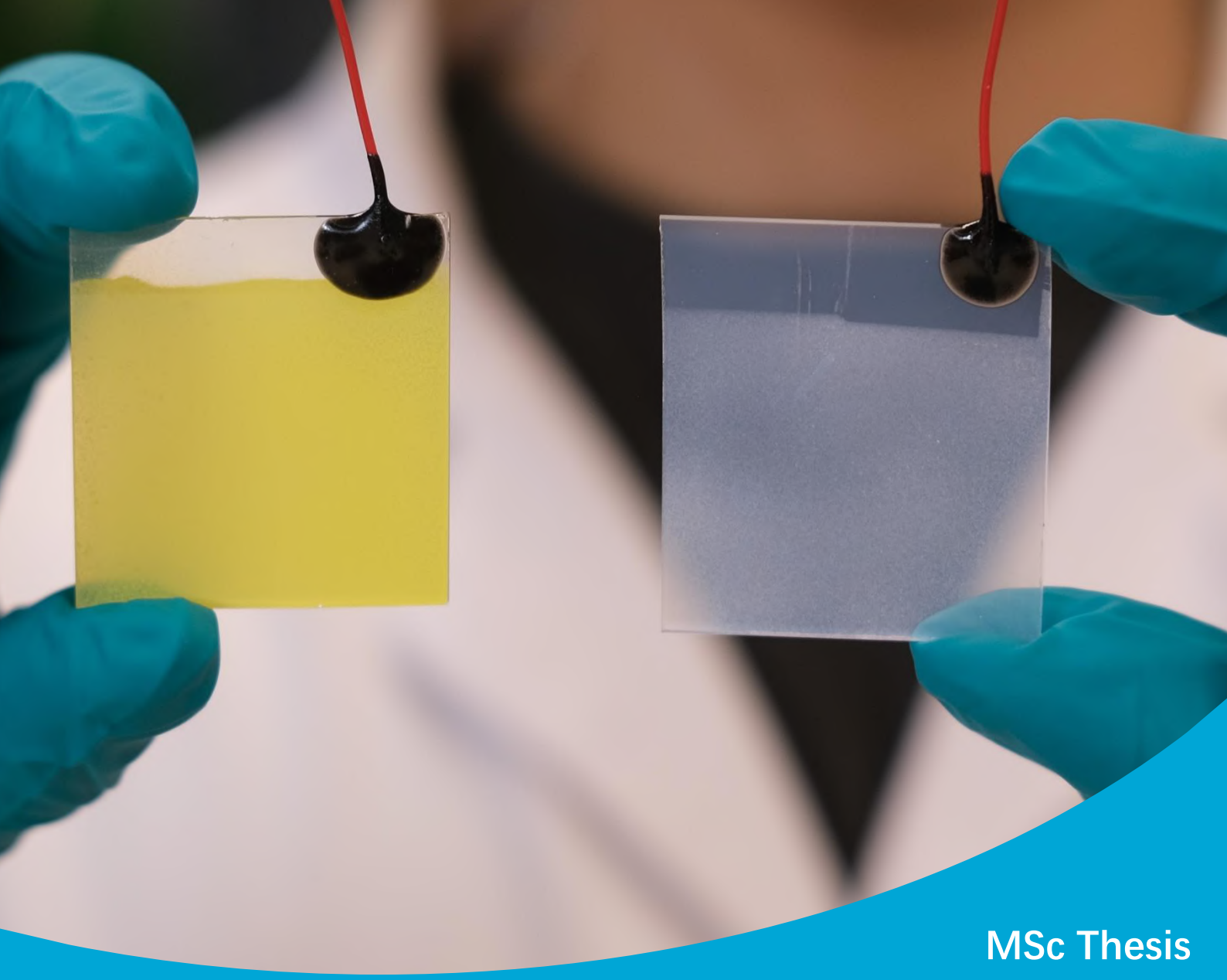

MSc Thesis

Photoelectrocatalytic degradation of organic micropollutants with $BiVO_4/(TiO_2/GO)_{mix}$ ternary composite photoanodes

Yuhao Wu

September 2022

TU Delft

Master of Science in Civil Engineering
(Track of Environmental Engineering)
Faculty of Civil Engineering and Geosciences
Delft University of Technology
The Netherlands

MASTER THESIS

Photoelectrocatalytic degradation of organic micropollutants with $BiVO_4/(TiO_2/GO)_{mix}$ ternary composite photoanodes

by
Yuhao Wu

15 September 2022

Assessment Committee Members:
Prof. Dr. Jan Peter van der Hoek
Dr. Ir. Henri Spanjers
Agha Zeeshan Ali

Acknowledgment

As I type the word 'Acknowledgements' on my keyboard, my two-year experience as a master student at the Delft University of Technology is also coming to an end. My mood at this moment is not as relaxed and happy as I expected, but some sad and emotional, because this is a crucial and precious memory in my life.

Firstly, I would like to extend my sincere thanks to my supervisors Prof. Dr. Jan Peter van der Hoek and Dr. Ir. Henri Spanjers for their continued support and encouragement throughout this project. At each meeting, they provided many constructive suggestions on my research process, presentation skills and writing style, which will still help me a lot during my future career. In addition, I want to express my gratitude to my daily supervisor Agha Zeeshan Ali. Throughout the research, he was always available to answer my questions, big and small, which helped me overcome several obstacles in the experiments. He is my supervisor but also my friend. I would also like to sincerely thank my colleague Yiqian Wu who started her thesis almost the same time as I did. We often discussed problems we met in our research together, and although there were occasional arguments, we could always solve them and make progress in the end. She also gave me solid moral support during the most difficult time of my PhD application. Thank you, Yiqian!

Furthermore, I would like to thank Dr. Ing. Kim Maren Lompe and Connie Au for supporting my experiments when I needed help at the most. Without your help, my experiments would not have been completed successfully and on schedule.

Last but not least, I would like to thank my parents in China for their unconditional love and support to let me pursue my dreams without any worries. I love you all!

The day I received the offer from TUD two years ago was one of the most exciting moments of my life. Now, two years later, I'm sitting at my computer typing these lines with tears in my

eyes. Yes, I did it, but I will never stop my steps. Strive for greatness!

Yuhao Wu

15 September 2022

Delft

Abstract

In the recent decade, a wide range of emerging contaminants (ECs) has been regularly detected in the wastewater treatment plants (WWTPs) effluent, surface water and even groundwater. Among all these ECs, organic micropollutants (OMPs) are receiving increasing attention due to their characteristics of low concentration, difficulty in degradation and their harmful effects on humans and the environment. Nineteen OMPs have been included on the contaminant watch list of the European Union Water Framework Directive since 2015 and efficient and reliable methods to eliminate them are researched worldwide. Therefore, in this study, five of these 19 OMPs (benzotriazole (BTA), carbamazepine (CBZ), diclofenac (DIC), ketoprofen (KET) and caffeine (CAF)) were selected as target OMPs. And the research objective is to fabricate a ternary composite photoanode and to investigate its photoelectrocatalytic degradation performance for all five target OMPs.

$BiVO_4$/(TiO_2/graphene oxide (GO))$_{mix}$ ternary composite thin films were successfully deposited on fluorine-doped tin oxide (FTO) glass substrates using ultrasonic spray paralysis (USP) method to form a ternary heterojunction structure and to improve the photoelectrocatalytic performance for degradation of the five target OMPs. The morphology, crystal phase, surface chemical composition, optical and electrochemical properties of this ternary composite photoanode were analyzed by scanning electronic microscopy (SEM), energy dispersive X-ray spectroscopy (EDS), X-ray diffraction (XRD), X-Ray photoelectron spectroscopy (XPS), UV-vis spectroscopy, incident photon-to-electron conversion efficiency (IPCE), linear sweep voltammetry (LSV) and electrochemical impedance spectroscopy (EIS), respectively. The results of these analyses showed that TiO_2 P25 nanoparticles and GO sheets were distributed uniformly on the brain-shaped $BiVO_4$ structure which indicated that the ternary heterojunction structure was formed successfully. From the UV-vis analysis, it could be estimated that the band gap energy

for $BiVO_4/(TiO_2/GO)_{mix}$ ternary composite photoanodes is 2.43 eV. Further, the LSV and EIS analysis showed that the photocurrent of the ternary composite photoanodes is lower than pure $BiVO_4$ photoanodes.

The degradation experiments were divided into five stages. The optimal photoanode type was first determined in the pre-experiment stage using methylene blue (MB) as indicator organic pollutant and then the effect of initial concentrations of target OMPs and initial pH on the degradation efficiency were studied in stage II and III, respectively. The highest removal efficiency of the five target OMPs was obtained with initial OMPs concentration at 10 $\mu g \cdot L^{-1}$ and initial pH range of 3.5-4.0. The degradation experiments were triplicated under this optimal condition in stage IV. It was noticed from the results that the degradation efficiency of different OMPs after 3 hours of reaction time varied from 31.1 % to 99.5 %. To further confirm that there is competition between the five target OMPs during the photoelectrocatalytic degradation process, experiments were carried out in which individual OMPs were degraded independently. The reusability and stability of the photoanodes were evaluated in stage V. Trapping experiments using scavengers were also included in this stage, which showed that superoxide anions was the most active species during the degradation process.

Keywords. organic micropollutants, photoelectrocatalysis, ultrasonic spray paralysis, ternary composite photoanodes, $BiVO_4$, TiO_2, graphene oxide, scavengers.

Nomenclature

0.1 List of Attributions

ECs	Emerging Contaminants
$WWTPs$	Waste Water Treatment Plants
$PFAS$	Polyfluoroalkyl Substance
$OMPs$	Organic Micro-Pollutants
ASP	Activated Sludge Process
MBR	Membrane Bioreactors
$MBBR$	Moving Bed Biofilm Reactors
$PPCPs$	Pharmaceuticals and Personal Care Products
SRT	Solids Retention Time
MF	Microfiltration
UF	Ultrafiltration
NF	Nanofiltration
RO	Reverse Osmosis
FO	Forward Osmosis
$MWCO$	Molecular Weight Cutoff
GO	Graphene Oxide
MB	Methylene blue
$LC-MS$	High performance liquid chromatography combined with tandem mass spectrometr
$AOPs$	Advanced Oxidation Processes
PEC	Photoelectrocatalysis
VB	Valence Band

CB	Conductive Band
ROS	Reactive Oxidative Species
USP	Ultrasonic Spray Pyrolysis
$PhACs$	Pharmaceutical Compounds
FTO	Fluorine-doped Tin Oxide
ITO	Indium Tin Oxide
SEM	Scanning Electron Microscopy
EDS	Energy Dispersive X-ray Spectroscopy
XRD	X-ray Diffractometry
XRF	X-ray Fluorescence
XPS	X-ray Photoelectron Spectroscopy
$IPCE$	Incident Photon to Current Efficiency
LSV	Linear Sweep Voltammetry
EIS	Electrochemical Impedance Spectroscopy
RGO	Reduced Graphene Oxide

0.2 List of Organic Micropollutants

BTA	Benzotriazole
CBZ	Carbamazepine
DIC	Diclofenac
KET	Ketoprofen
CAF	Caffeine

Contents

List of Figures

List of Tables

Chapter 1

Introduction

1.1 Organic Micropollutants

The demand for clean water continues to increase due to climate change, population growth, industrialization and environmental pollution, making the water stress on human society get heavier. To release the water scarcity threat, some water matrices such as wastewater treatment plants (WWTPs) effluent are considered a key factor [1, 2]. However, one of the key problems with direct and indirect water recycling reuse is the risk posed by emerging contaminants (ECs) at trace concentrations, including per- and polyfluoroalkyl substances (PFAS) and organic micropollutants (OMPs) such as pharmaceuticals, personal care products, pesticides and etc [3, 4].

Among all these ECs, OMPs have received increasing attention because they can interfere with human hormones, cause antibiotic resistance, and transform into more toxic products [5, 6]. Most of the OMPs are not completely removed in the WWTPs effluent [7, 8] and have been measured regularly in the water supply networks using surface water and groundwater as water source in the last decades, because the treatment processes of current WWTPs are not designed to treat OMPs, and there are few regulations or standards for them nowadays [6, 9]. The concentrations of OMPs in the environment are usually very low, typically in the range of ng$\cdot L^{-1}$ to μg$\cdot L^{-1}$, and therefore they are less likely to cause acute toxicity and adverse effects on humans during exposure [3, 4, 6, 9]. However, the risks of OMPs to the environment and human health are real due to their adverse effects on aquatic life and their long-term enrichment through the food chain [10, 11]. This study will therefore focus on efficient methods to remove OMPs. In this

section, the sources of OMPs in the environment and the target OMPs selected for this study will be elaborated on.

1.1.1 Source of Organic Micropollutants

Understanding the sources and existing types of OMPs in WWTPs effluent is essential for studying of efficient treatment technologies to ensure a good and healthy state of the water environment and human beings.

A recent study by Tröger et al., (2020) investigated the occurrence of OMPs in the Göta Älv river which is Sweden's second-largest source water. The results showed that the types of OMPs contained in this drinking water source included pharmaceuticals, pesticides, PFAS and other compounds [12]. Sörengård et al. (2019), on the other hand, analysed the occurrence and source of OMPs in the Fyris catchment in Sweden and concluded that wastewater was identified as the major source of various OMPs for the recipient River Fyrisr. In addition, hospital wastewater proved to be an important source of certain categories of OMPs such as antibiotics and antidepressants [13]. In a study conducted by Sánchez-Avila et al. (2012), it was also shown that river water and sewage treatment plant discharges to the sea were identified as the main sources of OMPs in coastal waters of the north-western Mediterranean [14]. Moreover, in a monitoring study investigating an urban catchment in southwest Stuttgart, Germany, Launay et al. (2016) reported that integrated sewer overflows and rainwater represent important pathways for various OMPs from the wastewater system to urban receiving waters [15]. Finally, in research which set out to study the risks and impacts of greywater reuse, Turner (2019) found that subsurface greywater irrigation practices can cause OMPs pollution to shallow groundwater and nearby surface water [16].

In summary, WWTPs effluent is the most significant contributor to total OMP emissions in the water body, with hospital wastewater, industrial wastewater and rainwater also contributing to some specific OMPs. The OMP types most often measured mainly include pharmaceuticals, pesticides and other compounds.

1.2 Current Technologies for Organic Micropollutants Removal

As mentioned in the previous section, various OMPs widely occur in drinking water sources through multiple pathways, such as WWTPs effluent, which pose considerable risks to human health and environmental safety. Therefore, technologies for OMP removal for both wastewater and drinking water treatment have been extensively studied recently. Some of the major treatment technologies are reviewed and discussed in this section.

1.2.1 Biological treatment processes

Biological treatment is often applied as a secondary treatment in conventional WWTPs. Its main mechanisms for removing pollutants, including OMPs, are physical adsorption, chemical transformation and biological degradation [17]. The main types of biological treatment include activated sludge process (ASP), biological trickling filters, membrane bioreactors (MBR), moving bed biofilm reactors (MBBR) [4]. One study by Kasprzyk-Hordern et al. observed the removal of 55 pharmaceuticals and personal care products (PPCPs) by ASP and biological trickling filter over a period of five months. The results showed the removal efficiency for most of these OMPs was only about 50 % [18]. In a study investigating MBR operated with a short solids retention time (SRT), Maeng et al. reported that OMPs such as carbamazepine and diclofenac could not be effectively removed, and the remove rate was strongly influenced by pH and temperature [19]. Therefore, although biological treatment has the advantages of cost saving, sustainability and environmental-friendly, its removal efficiency for OMPs is still minimal, and the water quality of the treated effluent is unsatisfacted.

1.2.2 Adsorption

Adsorption is often used as an advanced treatment after secondary treatment. Activated carbon adsorption is the most widely used type, including granular and powdered activated carbon. In a previous study, Guillosou et al. (2018) observed that activated carbon adsorption removed more than 50 % of the untreated OMP of the prior process [20]. However, the effectiveness of adsorption depends a lot on the physicochemical properties of the OMPs (e.g. molecular weight, pK_a, solubility, hydrophobicity and charge) and the adsorbent (e.g. polarity and surface properties). It is also worth noting that secondary contamination might happen if the saturated

adsorbent is not regenerated or disposed of properly [4].

1.2.3 Membrane separation technologies

Membrane separation technologies mainly include microfiltration (MF), ultrafiltration (UF), nanofiltration (NF), reverse osmosis (RO) and forward osmosis (FO), etc. The mechanisms of different membrane separation technologies are different. Membrane parameters such as the molecular weight cutoff (MWCO), membrane process type, membrane properties, fouling, operating conditions and physicochemical properties of the OMPs molecular largely determine the removal efficiency of the membrane separation process [4]. A wide range of OMPs can be removed by RO, NF and FO based on size exclusion mechanisms, while adsorption is the primary removal mechanism for UF because the molecular size of the OMPs is usually smaller than the MWCO value of the UF membrane [21]. Although good removal of certain OMPs, the main disadvantages of membrane separation technology are the rapid membrane fouling and the appropriate treatment of the concentrate generated in the membrane filtration process [4].

1.2.4 Advanced oxidation processes (AOPs)

Advanced oxidation processes (AOPs) are considered to be the technology that can fill the gap between the limitation of conventional treatments and the more exigent standards fixed by environmental regulations because conventional physicochemical and biological treatments are not effective in removing or breaking down OMPs. AOPs mainly include processes such as ozonation, UV/H_2O_2 oxidation process, wet oxidation processes and heterogeneous photocatalysis [22]. The mechanism of AOPs for OMPs removal usually consists of two steps, the first one is the in situ formation of reactive oxidative species (ROS) and the second one is the reaction happened between ROS and OMPs [23].

Ozonation is one of the most widely used AOPs for the treatment of wastewater containing OMPs. Ozonation can decompose OMPs directly by itself or indirectly by generating hydroxyl radicals. However, the ozonation process is very selective for electron-rich organic molecules [17]. In a study investigating the treatment for some OMPs using ozonation, Silva (2017) reported that the removal rates of bisphenol-A reached 60 % to 100 %, while for some highly resistant compounds such as bezafibrate, the removal efficiency was relatively low [24].

Heterogeneous photocatalysis is another AOPs that has been extensively studied for the removal of OMPs during the water and wastewater treatment. Heterogeneous photocatalysis driven by solar energy, in particular, has attracted significant attention in recent decades due to its cost and energy-saving advantages [25]. The mechanism is using wide band-gap materials as photocatalysts to generate electrons and holes and then further produce active species such as hydroxyl radicals and superoxide anions to react with OMPs when irradiated with photons of energy higher than the band-gap [26]. However, due to the very easy recombination of photogenerated electrons and holes, improvement strategies such as fabricating multiple heterojunction structures and applying a bias to avoid the recombination of holes and electrons effectively. Composite materials with matching band potentials are usually selected to form the heterojunction structure. Therefore, a contact electric field is formed at the heterojunction interface, which can transport the photogenerated electrons from one material to another, thus improving the separation efficiency [27]. It was proved that these strategies could improve the photocatalytic performance of the photocatalyst and enhance the degradation efficiency of OMPs [28–30]. Therefore, heterogeneous photocatalysis, especially photoelectrocatalysis is considered to be a very promising technique for OMPs treatment.

1.3 Photoelectrocatalysis of Organic Micropollutants

Photoelectrocatalysis (PEC) is a technique that combines photocatalysis and electrolytic. For classical photocatalysis, photocatalyst are used to generate electron/hole pairs under illumination, which produce active species on the surface of the electrodes and then degrade the OMPs. However, this process has a drawback of rapid recombination of photogenerated electron/hole pairs due to its low photonic efficiency. To solve this problem, the photocatalyst is made in a fixed form as a photoanode, and an external bias is added between it and the cathode, which produces the electric field to retard the recombination of electron-hole pairs and increase the lifetime of the generated holes and electrons [31]. During PEC process, electrons are transformed from the valence band (VB) of a material to the conductive band (CB), producing a positively charged hole. Many types of active species such as hydroxyl radical and superoxide radical are generated through a series of reactions of electrons and holes, which will degrade the OMPs near the electrodes. The mechanism of PEC is shown in Figure 1.1. It is worth noting that the irradi-

ation must have greater energy than that of the band gap of the material used as photocatalyst [32].

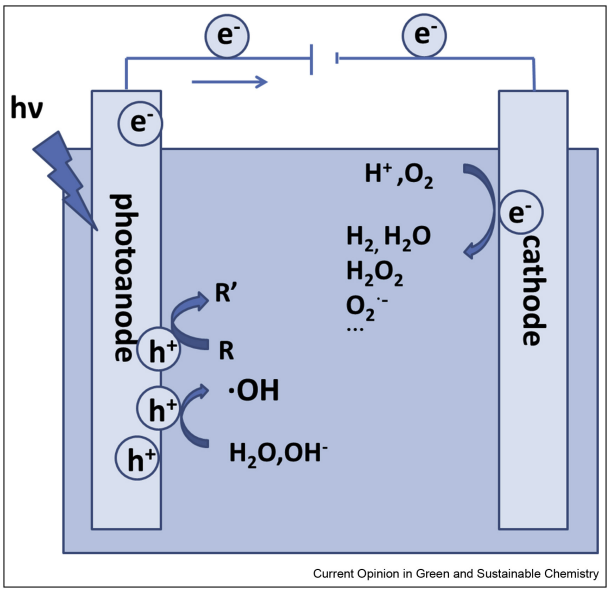

Figure 1.1: Mechanism of the PEC process for organics degradation. [33]

1.3.1 Photoelectrocatalysis using $BiVO_4$ photoanodes

Some requirements should be met by the materials before it can be used as photocatalyst with high efficiency in the PEC process, including efficient use of both UV light and visible light, low recombination rate of photogenerated electron/hole pairs and physical and chemical stability [34].

Materials such as TiO_2 [35], MoS_2 [36], WO_3 [37], Cu_2O [38] and ZnO [39] have been widely studied as promising photocatalysts for photoelectrocatalytic degradation of organic pollutants. Among them, $BiVO_4$ demonstrates potential due to its balance between features such as suitable bandgap energy, a proper band location, and high stability. The crystal structure of $BiVO_4$ greatly influences its properties. There are three common types: monoclinic scheelite, quadrate scheelite and quadrate zircon. Monoclinic $BiVO_4$ is a promising metal oxide photocatalyst with a band gap of 2.4 eV. Therefore, it can absorb visible light up to 525 nm [40]. Due to its excellent photocatalytic properties, $BiVO_4$ photocatalyst has been extensively applied for various purposes, including water splitting, photodegradation of various organic pollutants, etc. [41–43]. The mechanism of the photodegradation of OMPs by $BiVO_4$ photocatalyst is shown in Figure

1.2.

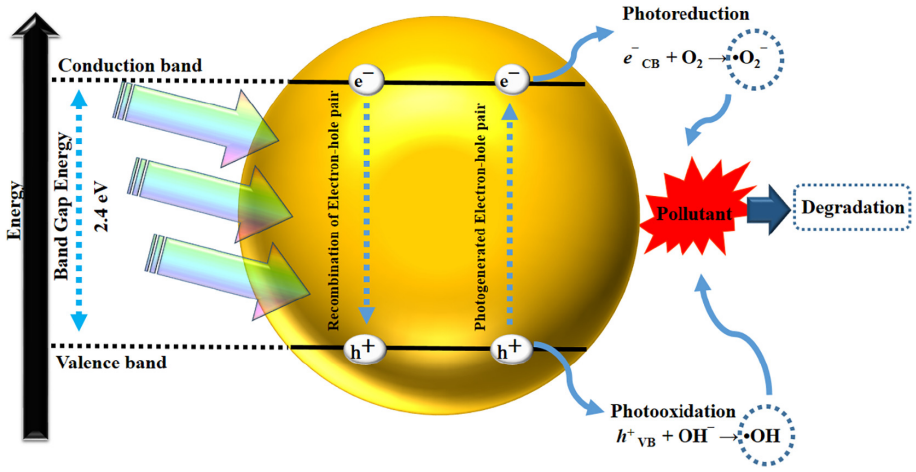

Figure 1.2: Photocatalytic degradation principle and mechanism of $BiVO_4$ photocatalyst. [44]

However, $BiVO_4$ still has some deficiencies in photo charge transfer, separation, and recombination rate, limiting its application as a high-efficiency photocatalyst [44]. To alleviate these problems, some studies have attempted to deposit $BiVO_4$ on substrates such as Fluorine-doped Tin Oxide (FTO) and Indium Tin Oxide (ITO) glass to fabricate photoanodes, and an external bias was added to the electrodes to form a PEC system [45]. In one study, Kiama et al. (2019) fabricated $BiVO_4$ thin films on FTO substrate by cyclic voltammetry deposition method and observed 93 % rhodamine B photoelectrocatalytic degradation within one hour with 1 V bias applied [45]. In another major study, Samsudin et al. (2020) synthesised $BiVO_4$ by simple hydrothermal treatment reaction and coated it on the FTO glass via the doctor blading method for photoelectrochemical water splitting from natural lake water [34].

1.3.2 Photoelectrocatalysis using $BiVO_4$-based photocatalyst

Another simple but effective strategy is to form a heterojunction structure to enhance the performance of $BiVO_4$-based photocatalysts in photonic efficiency, long-term stability and OMPs degradation efficiency [46]. Theoretically, the most important thing to form the heterojunction structure is the pairing between a low-to-mid-energy band gap material and high-energy band gap material, which will enhance light harvesting and improve the effective separation of photogenerated electron/hole pairs [29]. Heterojunction structures such as $BiVO_4$/BiOI [46], TiO_2/$BiVO_4$ [47], WO_3/$BiVO_4$ [48] and ZnO/$BiVO_4$ [40] have already been proved to have improved PEC

improved PEC activities over bare $BiVO_4$ photocatalyst for degradation of organic pollutants.

To further reduce the recombination rate of photogenerated electron/hole pairs and increase the adsorption towards OMPs of photoanodes, an elegant solid-state electrons mediator, graphene oxide (GO) has been introduced into the heterojunction structures in some studies [49, 50]. GO has the advantages of large specific surface area, high electron mobility and good thermal stability, so it can be added to form a binary or ternary composite photocatalyst. GO also has a large number of oxygen-containing functional groups, which can increase the adsorption to the photoanodes in the environment with multiple compounds [51].

By developing a novel heterojunction of $BiVO_4/TiO_2$/GO composite for the degradation of reactive blue 19, Zhu et al. (2017) has been able to show that it is a promising heterostructured semiconductor photocatalysts for the photocatalytic degradation of organic pollutant with higher photodegradation efficiency than both bare $BiVO_4$ and $BiVO_4/TiO_2$ photocatalyst [49]. Yang et al. (2020) used GOP25/FTO photoanodes for the photodegradation of PFAS and the results showed that GO played a essential role in transferring electrons from excited TiO_2 to GO thereby enhance the photocatalysis activity [50]. Therefore, this research focused on a ternary composite photoanode with the heterojunction structure of $BiVO_4$, TiO_2 and GO.

1.4 Thesis Structure

This report is composed of six themed chapters. Chapter 1 presents the background knowledge of this study. The necessity and conventional methods of removing OMPs are summarised through a literature review. The development and mechanism of $BiVO_4$-based photoelectrocatalysis are also included. The photoelectrocatalytic degradation of OMPs using $BiVO_4$-based composite photoanodes is considered an effective and promising technique to eliminate OMPs in the aquatic environment. However, there are some problems and research gaps during the current research, which are discussed in Chapter 2. This chapter also lays out the overall research objective, questions, and corresponding research approaches to answer the questions. Chapter 3 concerns the specific materials and methodology used for this study. The results of every experimental stage are discussed and analysed in Chapter 4. The conclusions, limitations and suggestions of this study are displayed in Chapters 5 and 6, respectively.

Chapter 2

Research Set-up

2.1 Knowledge Gap

Based on the literature review and discussion in Chapter 1, it is acknowledged that the excellent capacity of $BiVO_4$-based composite photocatalyst for the photodegradation of OMPs has drawn increasing attention and is identified as an effective and promising method. However, the following knowledge gaps remain speculative:

(1) Much of the research up to date tended to focus on photocatalysis degradation using photocatalysts in the form of slurry. The photoelectrocatalytic degradation of target OMPs using a fixed form of photocatalyst (photoanodes) is rarely reported.

(2) A search in the literature revealed few studies had identified efficient methods for making ternary composite photoanodes. In most studies, photoanodes are fabricated by the doctor blade method, electrodeposition and dip-coating methods, which suffer from the difficulty of fabricating on a large scale and controlling the quality of electrodes obtained.

(3) Information on the photoelectrocatalytic degradation behaviour of mixture of OMPs is lacking. In numerous studies, they are always individually observed.

(4) During photoelectrocatalytic degradation processes, the effect of operating conditions such as initial concentration and initial pH of OMPs solution on degradation efficiency have not been closely examined.

(5) The photoelectrocatalytic degradation feasibility and performance of multiple OMPs using ternary composite photoanodes in long-term processes are unknown.

(6) The reaction mechanism of the photoelectrocatalytic degradation process using the ternary composite photoanodes is understudied.

2.2 Research Objective

This study focuses on the degradation of OMPs in WWTPs effluent by photoelectrocatalysis. Based on the introduction chapter and the research gap section, the overall research objective of this study is:

To fabricate and characterise the ternary composite photoanode with $BiVO_4$, TiO_2 and GO, and to investigate its photoelectrocatalytic degradation performance in an aquatic environment with the five target OMPs and its feasibility in the long-term degradation process.

2.3 Research Questions

To achieve the above research objective, the following research questions were formulated.

(1) What is the optimal layer arrangement and characterization of the ternary composite photoanodes with $BiVO_4$, TiO_2 and GO?

(2) What is the photoelectrocatalytic degradation efficiency of organic pollutants using the ternary composite photoanode?

(3) What are the optimal starting operational conditions on the photoelectrocatalytic degradation process of the five target OMPs using the ternary composite photoanodes?

- What is the optimal initial concentration of target OMPs during the degradation experiments?
- What is the optimal initial pH of the target OMPs solution during the degradation experiments?

(4) What is the photoelectrocatalytic degradation feature and behaviour of target OMPs in a multiple OMPs environment.

(5) What is the photoelectrocatalytic degradation efficiency of target OMPs using the ternary composite photoanodes after two to three cycles of sequential degradation processes?

(6) What is the reaction mechanism of the photoelectrocatalytic degradation process using the ternary composite photoanodes?

2.4 Research Plan

The related research plan and approaches are listed in Table 2.1 to answer the above research questions.

Table 2.1: Research plan and approaches of the project.

Research Question	Research Stage	Research Approach
(1), (2)	Stage I	Stage I was a pre-experiment in which methylene blue was used as an indicator organic pollutant to investigate the feasibility of the fabricated ternary composite photoanodes in photoelectrocatalytic degradation and to determine its optimal layer arrangement. Then, several technologies were applied to characterize the photoanodes.
(3)	Stage II	With the determined layer arrangement of the photoanodes, stage II focused on the five target OMPs and investigated the effect of different initial OMPs concentrations on the degradation efficiency in a neutral environment.
(3)	Stage III	Stage III studied the effect of the initial pH of the environment on the degradation efficiency of 5 target OMPs and the pH value was recorded during degradation experiments.
(4)	Stage IV	In stage IV, firstly, degradation experiments of the five target OMPs using photolysis, $BiVO_4$ and the ternary composite photoanodes were conducted. And then, triplicate degradation experiments of target OMPs were performed under the optimal conditions. Finally, single OMP degradation experiments were conducted to study the degradation feature and behaviour of the target OMPs.
(5), (6)	Stage V	In stage V, firstly, the determined optimal operational conditions were applied in three cycles of photoelectrocatalytic degradation experiments of the five target OMPs to evaluate the feasibility and stability of prepared photoanodes in the long-term degradation process. Secondly, trapping experiments using several scavengers were carried out to study the active species involved in the photoelectrocatalytic degradation of OMPs.

Chapter 3

Materials and Methods

3.1 Materials

$Bi(NO_3)_3{\cdot}5H_2O$, acetic acid, nitric acid, sodium hydroxide and $VO(AcAc)_2$ were purchased from Sigma-Aldrich (USA). p-Benzoquinone was purchased from Thermo Scientific (USA).

Nano graphene oxide (GO) were purchased from Suzhou Tanfeng Graphene Technology Co., Ltd. (China), whereas Degussa P25 TiO_2 nano powder was purchased from Tianjin Baima Technology Co., Ltd. (China). The fluorine-doped tin oxide glass substrate was purchased from Luoyang Guluo glass Co., Ltd. (China). Methylene blue used in the pre-experiment as an indicator pollutant was purchased from CZTL (UK).

3.1.1 Selected Organic Micropollutants

Five representative OMPs were selected as target OMPs in this study based on their properties, details of which are listed in the Table 3.1. Benzotriazole (BTA) is a corrosion inhibitor used to decrease the corrosion rate of metals and alloys and it is considered to be an emerging pollutant due to its persistence, bioaccumulation and toxicity [52]. Carbamazepine (CBZ) is an anticonvulsant drug used to treat epilepsy and neuropathic pain. Diclofenac (DIC) is widely used analgesics and anti-inflammatory drugs [53]. It may accumulates in the environment causing long-term pollution [54]. Ketoprofen (KET) is a nonsteroidal anti-inflammatory drugs with analgesic and antipyretic effects and it may cause health risk to human [55]. Caffeine (CAF) is used to produce a variety of medicines, consumed beverages and food products as an elementary

compound. Therefore, it can be frequently detected at high concentrations in the surface waters, groundwaters and WWTP effluent worldwide [56]. The stated five OMPs were chosen for this study and they are placed in the contaminant watch list clarified by European Union Water Framework Directive [17, 57].

Technical grade CAF, CBZ, DIC, BTA and KET were purchased from Sigma-Aldrich (USA).

Table 3.1: Five selected organic micropollutants and their parametrs.

OMPs	Formula	CAS	pK_a	Charge (pH 7)
Benzotriazole (BTA)	$C_6H_4N_3$	95-14-7	8.37	+
Carbamazepine (CBZ)	$C_{15}H_{12}N_2O$	298-46-4	13.9	0
Diclofenac (DIC)	$C_{14}H_{10}Cl_2NNaO_2$	15307-86-5	4.15	-
Ketoprofen (KET)	$C_{16}H_{14}O_3$	22071-15-4	4.45	-
Caffeine (CAF)	$C_8H_{10}N_4O_2$	58-08-2	14	+

3.2 Methods

3.2.1 Film Preparation

The transparent $BiVO_4$ thin film and TiO_2/GO thin film were deposited on an FTO glass surface (40mm x 40mm, 7 Ω/square, Luoyang Guluo glass Co., Ltd., China) by ultrasonic spray pyrolysis method as shown in Figure 3.1. The FTO glasses were first ultrasonicated in acetone for 5 minutes and then rinsed by demineralised water to clean the surface. The spray precursor solution for $BiVO_4$ film was prepared as following. 0.02 M $Bi(NO_3)_3{\cdot}5H_2O$ (99% Sigma Aldrich) was dissolved in 10 mL acetic acid (98% Sigma Aldrich) and an equimolar amount of $VO(AcAc)_2$ (99% Sigma Aldrich) was dissolved in 20 mL demineralised water and ethanol mixture. The ratio between water and ethanol was 1 : 1. The precursor solution was then made by mixing above solutions together slowly to form a clear blue homogenous solution. The spray coating process was controlled by an ultrasonic spray system. A multistage X-Y axis CNC controller (MSK-USP-ST1, MTI Corporation, USA) was adopted in this system to control the progressive scanning motion of the nozzle using a set of programmed X–Y linear motion stages. The distance between the titanium alloy cylindrical spray nozzle and the substrate was 10 cm and the FTO substrate was kept at 300 °C on a hot plate (EQ-HP-1515-LD, MTI Corporation, USA) in an open atmosphere. The nozzle was fixed to a 0.05 W digital ultrasonic generator (MSK-SP-01A, MTI Corporation, USA) and the feeding rate of the precursor solution was set to 0.3 $mL{\cdot}h^{-1}$

by a syringe pump (NE-1010, ProSense B.V., the Netherlands). The pressure of the compressed air acting as a carrier gas was fixed at 0.25 bar. The spray coating process was conducted twice to form the homogeneous nanostructured $BiVO_4$ film. Subsequently, the prepared $BiVO_4$ photoanodes were further annealed at 460 °C for 2 h with climbing rate of 2 °C per minute.

To prepare the spray precursor solution for TiO_2/GO film, 0.001 M nano GO (Suzhou Tanfeng Graphene Technology Co., Ltd., China) was first dispersed in 30 mL demineralised water and ethanol mixture and ultrasonicated for 1 h. The ratio between water and ethanol was 1 : 9. Then 0.02 M P25 TiO_2 nano powder (Tianjin Baima Technology Co., Ltd., China) was addded into the above mixture and then stirred for 2 h and ultrasonicated again for 1 h. The spray coating method was the same as the $BiVO_4$ film, except that the temperature of the heating plate was 150 °C. Finally, the prepared electrodes were annealed at 500 °C for 1 h in the oven with climbing rate of 5 °C per minute and used for further characterizations and degradation experiments.

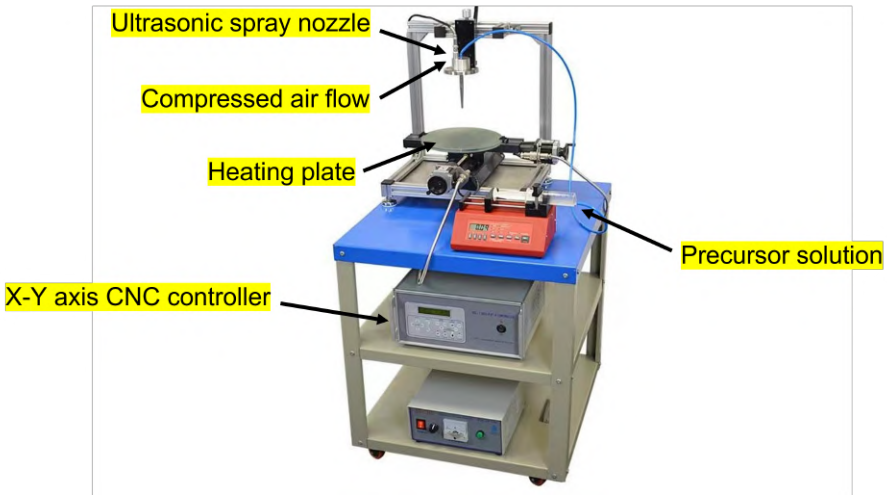

Figure 3.1: Ultrasonic spray pyrolysis equipment.

3.2.2 Film Characterization and Photoelectrochemical Measurement

The morphology and microstructures of the photoanodes were studied by scanning electron microscopy (SEM) using FEI Model Quanta 650 Field Emission Scanning Electron Microscope coupled with energy-dispersive X-ray spectrometer (EDS) using Inca 250 SSD XMax20 detector. The crystalline phases and purity analysis of the as-prepared photocatalyst film was conducted by X-ray diffraction (XRD) and X-ray fluorescence (XRF) using a Bruker D8 Advance diffractometer

(Bruker, USA) at 45 kV and 40 mA in a Bragg–Brentano configuration with Cu Kα radiation. Xray photoelectron spectroscopy (XPS) analysis was carried out with a Thermo Fisher K-Alpha surface analysis machine (Thermo Fisher Scientific, USA).

UV–vis absorbance spectra (LAMBDA 1050+ UV/Vis/NIR spectrophotometer, UV Winlab software) and incident photon-to-electron conversion efficiency (IPCE) were used to analyse the optical properties of the prepared photoanodes with the wavelength range from 280 to 800 nm.

As for the electrochemical properties study, linear sweep voltammetry (LSV) was conducted with potential from -0.2 V_{REF} to 1.5 V_{REF} and scan rate of 0.1 V/s. Electrochemical impedance spectroscopy (EIS) was also applied in the five target OMPs solution under both dark and light condition with applied frequency from 10000 Hz to 0.01 Hz.

3.2.3 Degradation Experiments Setup

The photoelectrocatalytic degradation experiments of methylene blue and five OMPs were conducted on an electrochemical workstation (Autolab B.V., AUT85176, The Netherlands). As shown in Figure 3.2, the degradation reactor was a 175 mL two-electrode cube quartz cell with the prepared photoanode and carbon stick employed as the working electrode and counter electrode. During the degradation process, the reactor was placed in a solar simulator (Atlas, SUNTEST XXL+, USA) and the irradiation sources were three Xenon lamps (1700 W) to obtain a irradiance of 60 W/m^2 from directly above.

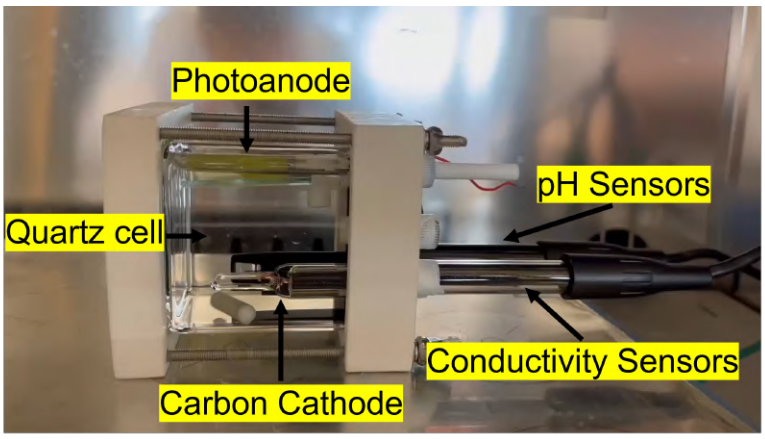

Figure 3.2: The two-electrode quartz reactor configuration during photoelecrocatalytic degradation process. Photoanode on the top connected the working electrode and a carbon stick connected the cathode electrode.

3.2.4 Preparation of solutions

The preparation work before the degradation experiments included preparing methylene blue and target OMPs stock solution and cleaning the experiment materials.

0.25 g methylene blue powder was added into 500 mL demi water to prepare the methylene blue stock solution at the concentration of 50 $mg \cdot L^{-1}$. During the pre-experiments, this stock solution was spiked into demi water at a target concentration of 2.5 $mg \cdot L^{-1}$ and then used. For the main experiments, 10 mg of each five selected OMPs were dissolved in 1 L demi water to obtain a five-OMPs stock solution at the concentration of 10 mg/L. Then, this stock solution was spiked into demi water at a target concentration of 10, 20, 40 $\mu g \cdot L^{-1}$ for the initial concentration investigation. As for the experiments studying the effect of initial pH, the pH was adjusted to target range of 3.5-4.0, 6.5-7.0, 8.5-9.0 using HNO_3. Due to different water solubility, a stock solution containing these OMPs was first prepared at the concentration of 10 $mg \cdot L^{-1}$. All the prepared stock solutions were stored in the fridge at the temperature below 5 °C to keep them in a stable condition.

3.2.5 Cleaning procedure

After every spray coating process, the nozzle and connected tube were first cleaned with 30 mL HNO_3 solution and then continued to rinse them with acetone and demi water for three times. Finally, they were air-dried for the next use.

All the glass wares including the quartz reactor for degradation experiment, graduated cylinder, beaker and volumetric flask were first cleaned using soap and a brush and then rinsed with demi water. Finally, they were rinsed with ultra-pure water and then air-dried for use.

3.2.6 Stage I: Pre-experiments

To test the degradation effect of different materials on organic pollutants in water and determine the best arrangement of the ternary composite photocatalyst, six types of photoanodes were prepared as listed in Table 3.2.The materials of photoanode 1 and 2 were pure $BiVO_4$ and TiO_2, respectively. Photoanode 3 had two different layers with one $BiVO_4$ layer deposited on FTO glass and one TiO_2 layer on top of it. As for photoanode 4, a thin film of mixture of TiO_2 and GO was deposited on the substrate. Photoanode 5 and 6 were two different layer

arrangment of the ternary composite photoanodes. $BiVO_4/(TiO_2/GO)_{mix}$ means $BiVO_4$ layer was at the bottom and TiO_2/GO mixture layer was on the top, while the arrangement order of $(TiO_2/GO)_{mix}/BiVO_4$ photoanode was opposite. Figure 3.3 shows how these photoanodes look like. Methylene blue was used as an indicator organic pollutant in the pre-experiments because its absorbance can be quickly measured by UV-vis spectrophotometer and then its concentration can be calculated according to the calibration curve.

Table 3.2: Six photoanodes used in the pre-experiment with different materials and arrangement

Number	Material and arrangement
1	$BiVO_4$
2	TiO_2
3	$BiVO_4/TiO_2$
4	$(TiO_2/GO)_{mix}$
5	$BiVO_4/(TiO_2/GO)_{mix}$
6	$(TiO_2/GO)_{mix}/BiVO_4$

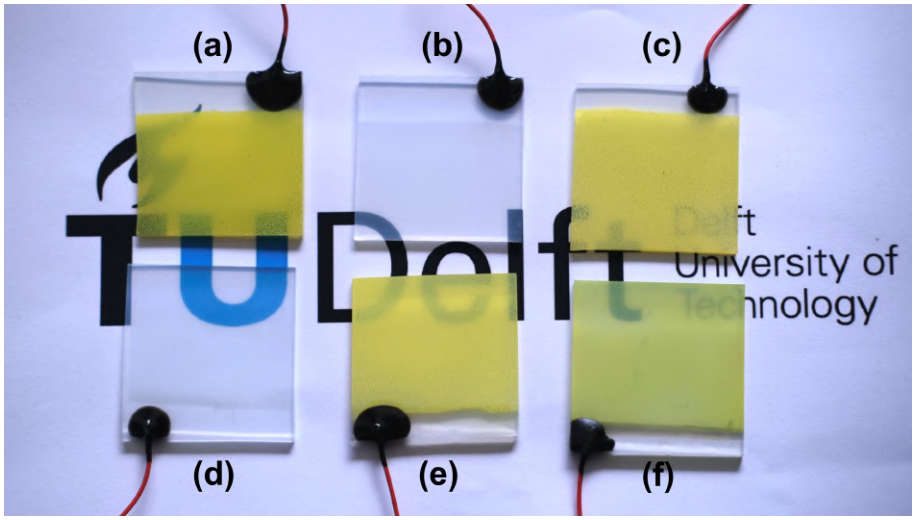

Figure 3.3: Photographs of the photoanodes: (a) $BiVO_4$, (b) TiO_2, (c) $BiVO_4/TiO_2$, (d) $(TiO_2/GO)_{mix}$, (e) $BiVO_4/(TiO_2/GO)_{mix}$, (f) $(TiO_2/GO)_{mix}/BiVO_4$.

Before the degradation experiments, the methylene blue stock solution was spiked into 2.5 $mg{\cdot}L^{-1}$ with 0.1 M of Na_2SO_4 as the electrolyte and then 150 mL this solution was loaded into the quartz reactor. The electrode was soaking and stirred in dark for 15 min to reach the adsorption-desorption equilibrium before the photoelectrocatalytic degradation process. Then, the photoanode and cathode were connected to the electrochemical workstation and a bias voltage of 1 V was applied. After switching on the magnetic stirrer in the degradation reactor and solar

simulator, the photoelectrocatalytic degradation process started. Every batch run for 1 h, with 1.5 mL samples taken at 15 minutes intervals by pipette. All samples were individually loaded into cuvettes and cooled to room temperature in the dark before absorbance measurements were conducted.

After analysing and comparing all the degradation efficiency data of these six electrodes, the optimal arrangement of the ternary composite photocatalyst was determined and used for the following stages.

3.2.7 Stage II: Initial Concentration Experiments

After knowing the optimal material arrangement order of the photoanodes, the effect of the initial concentration of the OMPs solution on the degradation efficiency was investigated at this stage. Three initial concentrations were selected: 10, 20, 40 $\mu g/\cdot L^{-1}$, in multiples of 2. The 10 mg/L stock solution with 5 target OMPs was spiked into demi water to get the target concentrations with 0.1 M of Na_2SO_4 as the electrolyte. The initial pH was kept around 6-7 to have a neutral environment. The remaining experimental operations and procedures were consistent with the pre-experiments. Solution pH and conductivity during degradation experiments were observed in real time by a multifunctional water quality tester (M852, Bante Instruments Co., Ltd., China) and recorded at 15 minute intervals. Every batch run for 3 h, with 1 mL samples taken at 30 minutes intervals by pipette.

After analysing and comparing all the degradation efficiency data obtained with three target concentrations, the concentration with the highest degradation efficiency was chosen as the initial OMPs solution concentration for the initial pH study in stage III.

3.2.8 Stage III: Initial pH Experiments

The experiments to study the effect of initial pH on the degradation efficiency of the target OMPs were carried out on the basis of the initial concentration with the highest degradation efficiency derived in stage II. Three initial pH conditions were used: 3.5-4.0, 6.5-7.0, 8.5-9.0. Since the neutral initial pH condition was studied in the previous phase, only the acidic and basic initial pH condition were studied in this stage. Nitric acid (70% Sigma Aldrich) and sodium hydroxide (98% Sigma Aldrich) were used to adjust the initial pH of the OMPs solution before degradation

experiments. The remaining experimental operations and procedures were strictly consistent with the initial concentration experiments.

After analysing and comparing all the degradation efficiency data obtained under three target initial pH conditions, the initial pH value with the highest degradation efficiency was determined. Therefore, the optimal condition for the five target OMPs degradation was obtained. The degradation experiments under this condition were repeated two more times to ensure reproducibility of the experiments.

3.2.9 Stage IV: Triplicate & Single OMP degradation Experiments

Degradation experiments of the mixture of five target OMPs using direct photolysis, $BiVO_4$ and the ternary composite photoanodes were conducted under the optimal initial experimental conditions determined in the previous stages. Then the experiments with best degradation results were triplicated to calculate the standard error and verify the reliability of the data. Finally, single OMP degradation experiments were performed under the same conditions using the ternary composite photoanodes and the results were compared with that of multiple OMPs degradation experiments to study the degradation behaviour of each OMP.

3.2.10 Stage V: Reusability & Trapping Experiments

The reusability and stability of the photoanodes was evaluated by conducting the recycle experiments with the mixture of five target OMPs under the same reaction condition. The condition (initial concentration and initial pH) with the highest OMPs degradation efficiency was adopted and the electrode was recycled three times in this stage. In addition, in order to reveal the reaction mechanism of the photoelectrocatalytic degradation process using the ternary composite photoanodes, trapping experiments using p-benzoquinone and methanol as scavengers were completed. The concentrations of these two scavengers were both 5 mM.

3.2.11 Analytical Methods

In the pre-experiments, a calibration curve of methylene blue was first made as shown in Appendix. After degradation, the concentration of methylene blue was obtained by measuring its absorbance using a UV-vis spectrophotometer and then calculating based on the calibration

curve.

The concentration of target OMPs in the samples was measured by high performance liquid chromatography combined with tandem mass spectrometry (LC-MS). All Samples were first filtered with 0.2 μm glass fiber filters (GF-75, ADVANTEC®, Japan) and then diluted using ultrapure water. Then, 495 μL of this solution and 5 μL of internal standard calibration solution were added to the LC-MS sample vials. After mixing, the quantification of the five target OMPs in the samples was accomplished by the LC-MS devicde (Waters Acquity™, USA).

After obtaining the concentration of the contaminant in the sample, the degradation efficiency was calculated by the equation below. In the degradation experiments, the degradation efficiency were used to measure the photoelectrocatalytic degradation performance of the photoanodes.

$$Degradation\ \ Efficiency\,(\%) = (1 - \frac{C}{C_0}) \times 100 \tag{1}$$

C — Contaminant concentration in the sample.

C_0 — Initial contaminant concentration.

Chapter 4

Results and Discussion

4.1 Film Characterization

4.1.1 X-ray diffraction analysis

The phase composition of all the as-prepared photoanode samples was characterized by XRD and the XRD diffraction patterns of pure GO, pure $BiVO_4$, $(TiO_2/GO)_{mix}$, and $BiVO_4/(TiO_2/GO)_{mix}$ thin films photocatalyst are shown in Figure 4.1. The diffraction pattern of pure $BiVO_4$ sample exhibits fourteen broad peaks with 2θ value at 18.8°, 19.1°, 29.0°, 30.6°, 34.6°, 35.3°, 39.9°, 42.5°, 46.9°, 47.4°, 50.4°, 53.4°, 58.6°, 59.5° corresponding to the (101), (011), (112), (040), (200), (020), (211), (015), (204), (024), (220), (116), (312), (224) crystal planes of the monoclinic $BiVO_4$ phase (JCPDS Card No. 75-1867), respectively [58]. The XRD pattern of the $(TiO_2/GO)_{mix}$ sample shows peaks with 2θ value at 25.3°, 37.7°, 48.1°, 53.9°, 55.1°, 62.7° which are characteristics of (101), (004), (200), (105) (211), (204) crystal planes of anatase TiO_2 (JCPDS Card No. 88–1175), respectively. Furthermore, the diffraction pattern also has peaks at 27.4°, 36°, 41.2°, 56.6°, corresponding to (110), (101), (111) and (220) planes of rutile TiO_2 (JCPDS Card No. 84–1286), respectively [59]. Therefore, it can be analysed that the diffraction peaks of the prepared $BiVO_4$ photocatalyst was corresponding to a monoclinic clinobisvanite phase, while both anatase and rutile crystallites showed diffraction in the pattern of $(TiO_2/GO)_{mix}$. However, the XRD pattern of the pure GO sample does not show a peak around 10° as observed in previous study [60]. The reason might be that the concentration of GO precursor solution was too low or the sample was contaminated. As for the $BiVO_4/(TiO_2/GO)_{mix}$ sample, it can be clearly seen

that the diffraction peaks of both $BiVO_4$ and TiO_2 are observed in the $BiVO_4/(TiO_2/GO)_{mix}$ ternary composite photocatalysts without other detectable impurities. The intensities of diffraction peaks of both $BiVO_4$ and TiO_2 become weaker in the ternary composite photoanodes.

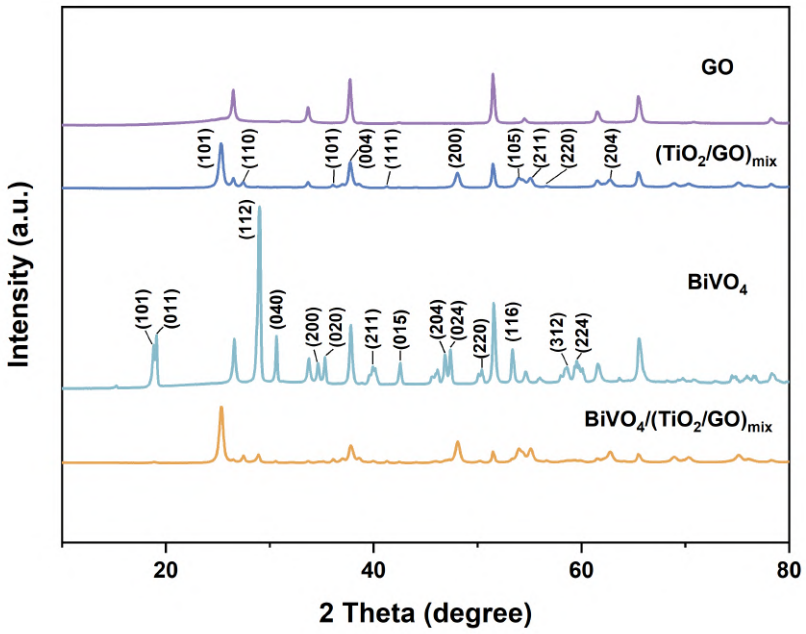

Figure 4.1: XRD patterns of the photoanodes: pure GO, pure $BiVO_4$, $(TiO_2/GO)_{mix}$ and $BiVO_4/(TiO_2/GO)_{mix}$.

4.1.2 Morphology measurement

The morphologies of all the as-prepared photoanode samples were characterized by SEM and the SEM images of bare FTO, pure $BiVO_4$, pure TiO_2, pure GO, $BiVO_4/TiO_2$ and $BiVO_4/(TiO_2/GO)_{mix}$ are displayed in Figure 4.2. For comparison, the morphology of the FTO substrate was first measured, as shown in Figure 4.2(a). The FTO surface showed microstructures with uniform-sized needle type grains and hillock shape [61]. As for $BiVO_4$ crystal (Figure 4.2(b)), brain-like structures in the size range of 0.2 to 0.5 μm were observed, which confirms the findings of previous researches using similar fabrication method [62, 63]. Figure 4.2(c) reveals that the TiO_2 photoanode sample shows a typical condensed spherical shape with the size in nanometer range which is consistent with previous studies [50]. Figure 4.2(d) shows the SEM image of GO with a flake-like structure before any treatment process. Only a small area of FTO substrate is covered

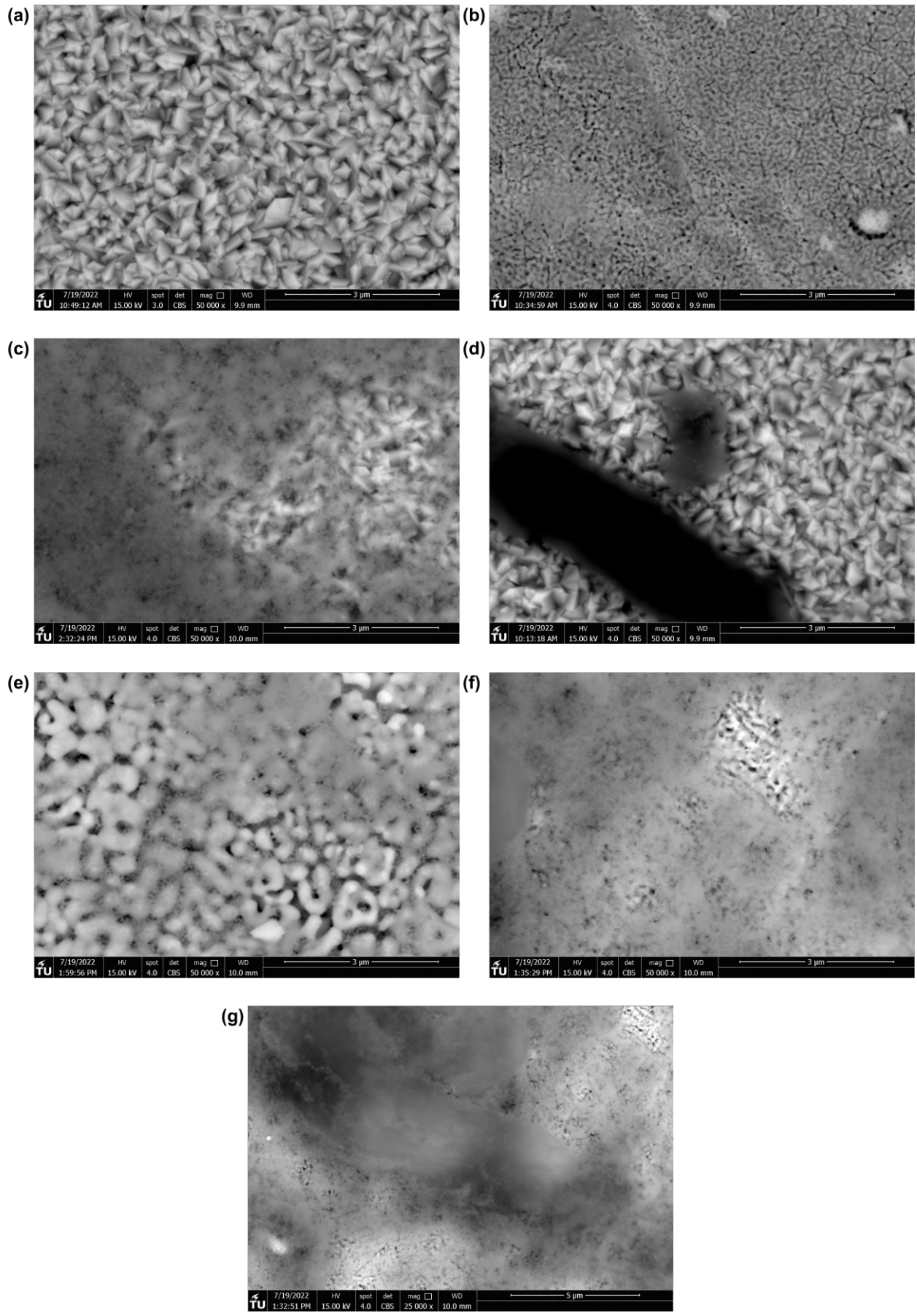

Figure 4.2: SEM images of 50000× (a) FTO, (b) $BiVO_4$, (c) TiO_2, (d) GO, (e) $BiVO_4/TiO_2$, (f) $BiVO_4/(TiO_2/GO)_{mix}$ and 25000× (g) $BiVO_4/(TiO_2/GO)_{mix}$.

by the GO sheet because of very low concentration of GO precursor solution. As can be seen in the $BiVO_4/TiO_2$ and $BiVO_4/(TiO_2/GO)_{mix}$ images (Figure 4.2(e) and (f)), the spherically shaped TiO_2 nanoparticles were dispersed uniformly on the $BiVO_4$ layer during the ultrasonic spray pyrolysis process. Figure 4.2(f) shows the SEM image of $BiVO_4/(TiO_2/GO)_{mix}$ with 25000 magnification. The $BiVO_4/TiO_2$ composite material was only covered by a small piece of GO sheet and the colour of GO sheet was lighter because the GO sheets broke under the high temperature of annealing and very low concentration of GO precursor solution [51].

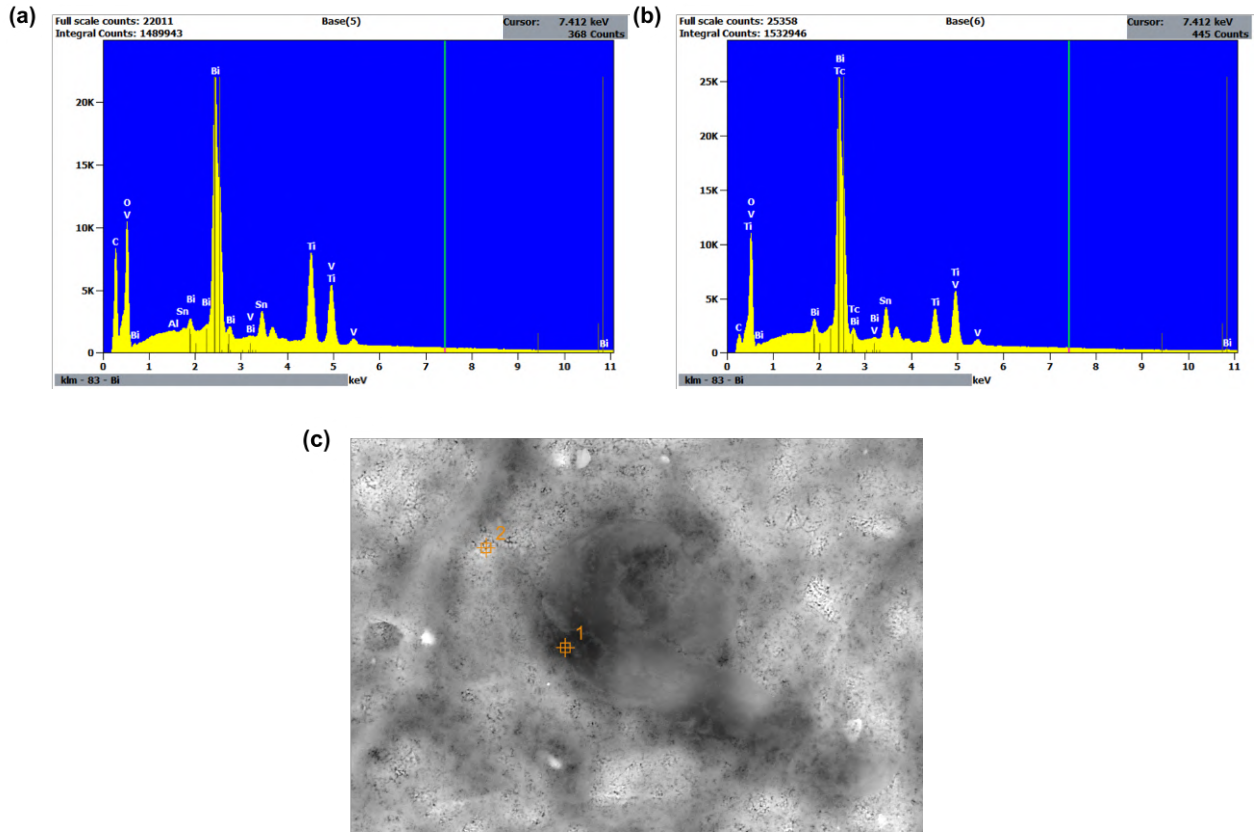

Figure 4.3: EDS spectrum of $BiVO_4/(TiO_2/GO)_{mix}$: (a) spot 1 (b) spot 2, (c) spots of measurement.

4.1.3 Energy dispersive X-ray spectroscopic analysis

Figure 4.3 shows the energy dispersive X-ray spectroscopic analysis for chemical composition of the as-prepared $BiVO_4/(TiO_2/GO)_{mix}$ photoanode sample at two different spots which can be found in Figure 4.3(c). Figure 4.3(a) represents the EDX result of the measurement at the dark flakes area on the sample (spot 1), while Figure 4.3(b) shows the result of the measurement at

a lighter area (spot 2). As Figure 4.3(a) and (b) show, the carbon peak measured at spot 1 is much higher than at spot 2 with 4.65 wt% and 0.94 wt% respectively, which further confirms the presence of GO on the $BiVO_4/(TiO_2/GO)_{mix}$ ternary composite photoanodes. Bi, V, Ti and O peaks were also observed, while the Sn peak comes from the FTO substrate.

4.1.4 X-Ray photoelectron spectroscopy analysis

XPS analysis was used to investigate the surface chemical composition and electronic state of pure GO, pure TiO_2, pure $BiVO_4$ and $BiVO_4/(TiO_2/GO)_{mix}$ composite photoanodes samples. Figure 4.4(a) shows the survey spectrum of all the samples, while Figure 4.4(b), (c), (d), (e) and (f) shows the core regional spectrum of Bi 4f, V 2p, Ti 2p, C 1s and O 1s in the composite photoanodes sample, respectively. Bi, V, Ti, O and C elements were detected in the XPS survey spectrum of $BiVO_4/(TiO_2/GO)_{mix}$ sample (Figure 4.4(a)). Two peaks Bi $4f_{5/2}$ at 163.48 eV and Bi $4f_{7/2}$ at 158.24 eV were obtained with the Bi 4f binding energy of the composite photoanodes (Figure 4.4(b)), which indicates that Bi existed in the sample prepared by ultrasonic spray pyrolysis method. As shown in Figure 4.4(c), there are two peaks at 529.18 eV and 516.19 eV in V 2p corresponding to V $2p_{2/1}$ and V $2p_{3/2}$, respectively. There are two peaks of Ti 2p at 463.78 eV and 458 eV which correspond to Ti $2p_{1/2}$ and Ti $2p_{3/2}$ (Figure 4.4(d)). The C 1s peaks presented at three positions with binding energies at 283.92 eV, 285.2 eV, and 287.83 eV which correspond to the graphitic carbon (C-C), carbon-hydroxyl/epoxy (C-O) and carbonyl (C=O) groups, respectively (Figure 4.4(e)). The intensity of C-C is much higher than that of C-O and C=O groups which indicates that a large amount of oxygen functional groups of GO were removed. The reason is that all those oxygen functional groups in the composite photoanodes were reduced to graphene under the high temperature of ultrasonic spray pyrolysis and annealing [64]. Two peaks were obtained for the O 1s binding energy with the peak at 529.19 eV corresponding to Ti–O binding energy and the peak at 530.16 eV corresponding to the surface oxygen deficiency binding energy or non-lattice oxygen [65, 66]. In conclusion, XPS spectras show that $BiVO_4$, TiO_2 and GO existed on the surface of the $BiVO_4/(TiO_2/GO)_{mix}$ ternary composite photoanodes.

To further confirm the existence of GO on the composite photoanodes, the core region of Ti 2p and O 1s in the $(TiO_2/GO)_{mix}$ and TiO_2 were compared in Figure 4.5. As Figure 4.5(a)

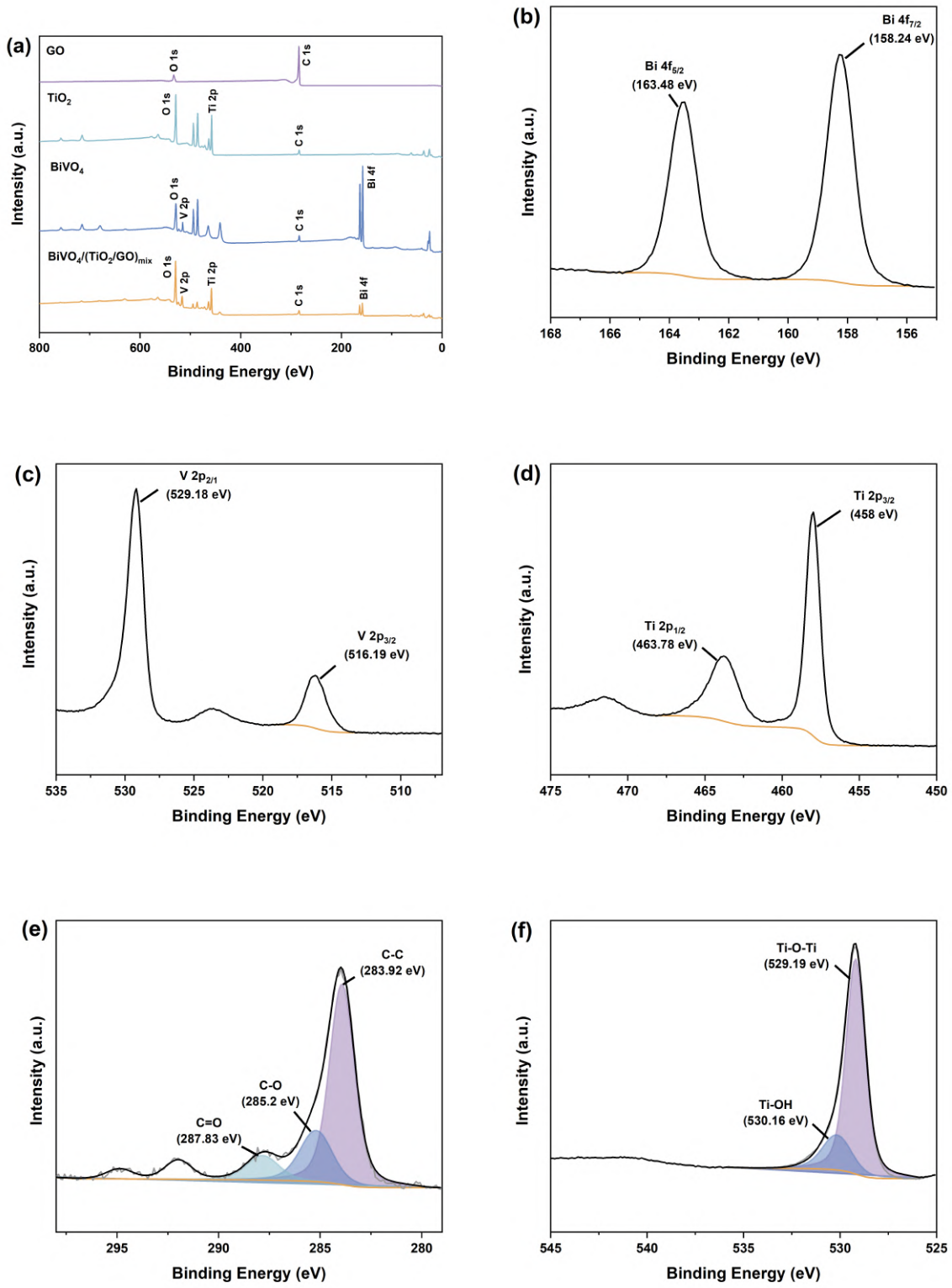

Figure 4.4: XPS spectra survey (a) of the $BiVO_4$, TiO_2, GO and $BiVO_4/(TiO_2/GO)_{mix}$ composite, and Bi 4f (b), V 2p (c), Ti 2p (d), C 1s (e), O 1s (f) core region spectra of $BiVO_4/(TiO_2/GO)_{mix}$ sample.

shows, the binding energy of Ti $2p_{1/2}$ and Ti $2p_{3/2}$ in $(TiO_2/GO)_{mix}$ shifted to a lower value (462.98 eV and 457.28 eV) as compared with those of pure TiO_2 (463.38 eV and 457.61 eV). As for the O 1s peak in $(TiO_2/GO)_{mix}$, Figure 4.5(b) shows that there was also 0.1 eV lower energy shift from 528.88 eV to 528.78 eV compared to pure TiO_2. The reason of these shifts is that the carbon atom has a larger electropositivity than the oxygen atom. Therefore, the binding energies of Ti 2p will decrease when Ti is coordinated with more carbon atoms than oxygen atoms which ravel the formation of the heterojunction between TiO_2 and GO [67]. The oxygen atom binding energy operates in a similar manner.

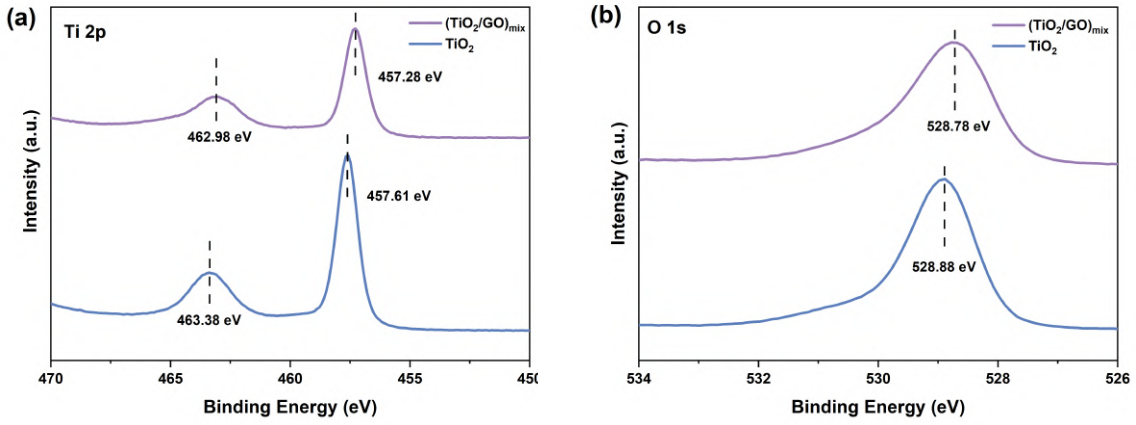

Figure 4.5: XPS spectra of $(TiO_2/GO)_{mix}$ and TiO_2: (a) Ti 2p spectrum, (b) O 1s spectrum.

4.1.5 UV–visible absorbance spectra analysis

Figure 4.6(a) shows the UV–visible absorbance spectra of as-prepared $BiVO_4$, TiO_2, GO, $(TiO_2/GO)_{mix}$ and $BiVO_4/(TiO_2/GO)_{mix}$ photoanodes. As can be seen, $BiVO_4/(TiO_2/GO)_{mix}$ ternary composite photoanodes outperformed $BiVO_4$, TiO_2, GO and $(TiO_2/GO)_{mix}$ in terms of optical absorption property in the range of 280–800 nm. In comparison with other samples, $BiVO_4/(TiO_2/GO)_{mix}$ also exhibited a strong red shift to longer wavelength regions in the visible light region between 400 and 800 nm, which indicates that the solar energy can be utilized more effectively. It could be attributed to the interaction between the free electrons on the TiO_2 and $BiVO_4$ surfaces and the unpaired π electrons of GO [49, 64, 68, 69]. From Figure 4.6(b), the band gap energy of $BiVO_4/(TiO_2/GO)_{mix}$, $(TiO_2/GO)_{mix}$, $BiVO_4$, TiO_2 and GO can be estimated to be about 2.43 eV, 3.23 eV, 2.45 ev, 3.32 eV and 3.68 eV from the plot of $(\alpha h\nu)^2$ versus photon energy $h\nu$. It is

kown that narrower band gap energy and broader absorbance in the region of visible light indicate a higher photocatalytic performance of photocatalyst [49]. Therefore, $BiVO_4/(TiO_2/GO)_{mix}$ ternary composite photoanodes exhibited a better optical properties than other samples.

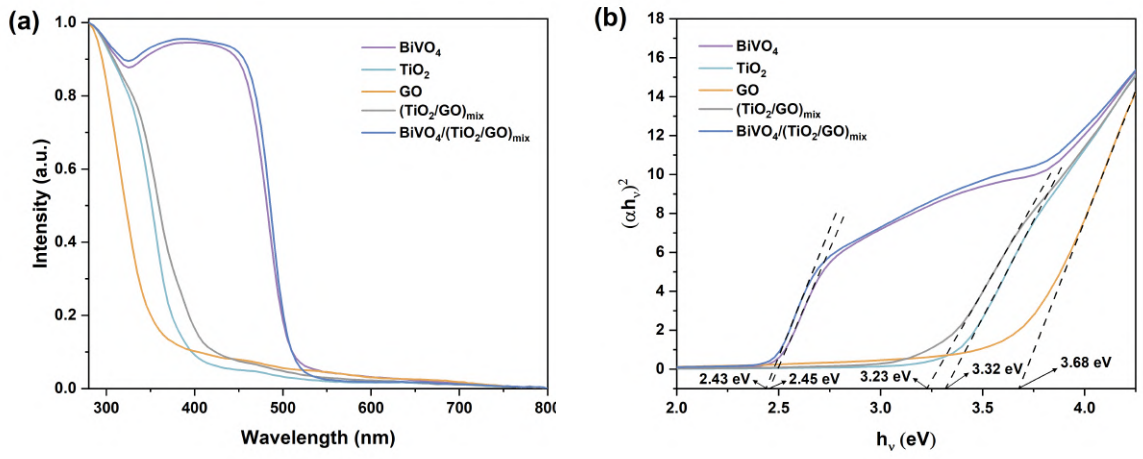

Figure 4.6: (a) UV–visible absorbance spectra and (b) Plot of $(\alpha h\nu)^2$ versus photon energy $h\nu$ of $BiVO_4$, TiO_2, GO, $(TiO_2/GO)_{mix}$ and $BiVO_4/(TiO_2/GO)_{mix}$ photoanodes.

4.1.6 Incident photon-to-current efficiency analysis

Incident photon-to-current efficiency was tested to show the light conversion efficiency of the ternary composite heterojunction of $BiVO_4/(TiO_2/GO)_{mix}$ and was compared to $BiVO_4$, TiO_2, GO and $(TiO_2/GO)_{mix}$ samples in Figure 4.7. TiO_2, GO and $(TiO_2/GO)_{mix}$ samples exhibited low efficiencies below 400 nm due to a large band gap. The IPCE of $BiVO_4$ reached about 18.2 % at 350 nm, while $BiVO_4/(TiO_2/GO)_{mix}$ had a slightly lower IPCE at nearly 17.0 % at 350 nm. The IPCE values of the samples were nearly zero around 550 nm, which is consistent with the UV-vis absorbance spectra results.

4.1.7 Linear sweep voltammetry and photocurrent density analysis

To test the photoelectrochemical response of the as-prepared photoanodes, the linear sweep voltammetry (LSV) was carried out in a 0.1 M Na_2SO_4 solution at the scan rate of 0.1 V/s and under back illumination for both dark and light conditions. The comparison of the current–potential plots of $BiVO_4/(TiO_2/GO)_{mix}$, $BiVO_4/TiO_2$, $BiVO_4$ and TiO_2 photoanodes is

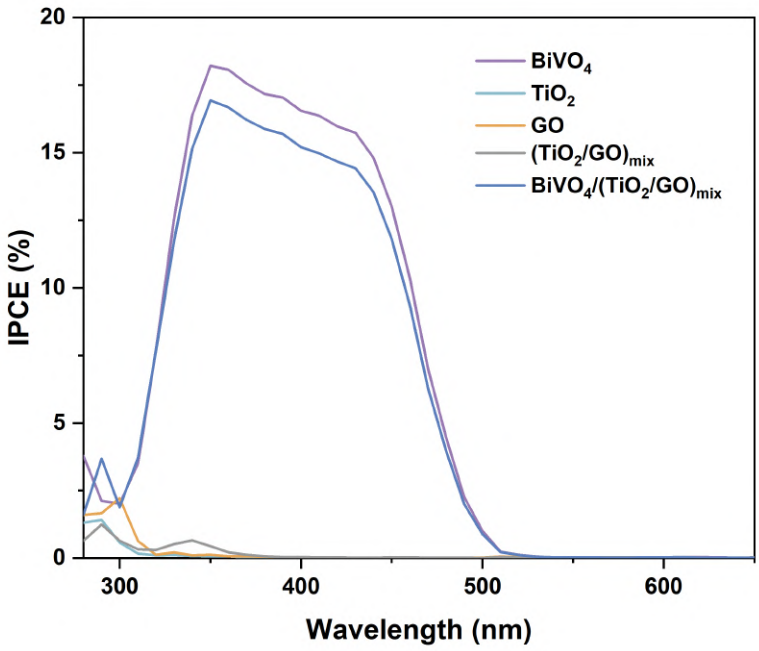

Figure 4.7: IPCE curve of $BiVO_4$, TiO_2, GO, $(TiO_2/GO)_{mix}$ and $BiVO_4/(TiO_2/GO)_{mix}$ photoanodes at the specified wavelength.

illustrated in Figure 4.8. The photocurrent of all the samples are close to 0 mA in dark and that of bare TiO_2 is also negligible because the efficient absorption of sunlight was hindered by its large band gap energy. The photocurrent density of $BiVO_4$ film under illumination was about 4.6 mA at 1 V, while the $BiVO_4/TiO_2$ sample exhibited a higher photocurrent density of 5.2 mA at 1 V. This result indicates that the combination of $BiVO_4$ and TiO_2 can reduce the recombination of photogenerated electrons and holes effectively due to the formation of the heterojunction structure. However, when GO is involved to form the ternary composite heterojunction structure, the photocurrent density decresed to 3.2 mA at 1 V, which shows that the performance of $BiVO_4/(TiO_2/GO)_{mix}$ photoanodes was not enhanced. Figure 4.9 shows the photocurrent generated by $BiVO_4$ and $BiVO_4/(TiO_2/GO)_{mix}$ photoanodes under irradiation during the degradation process. The photocurrent of $BiVO_4/(TiO_2/GO)_{mix}$ was slightly lower than that of bare $BiVO_4$ which is in line with the IPCE and LSV results.

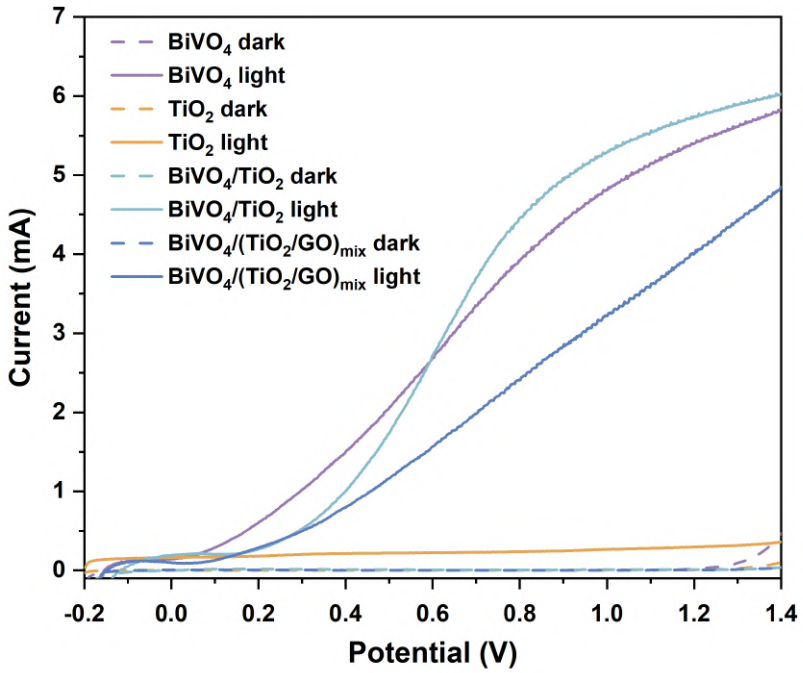

Figure 4.8: LSV plot of $BiVO_4$, TiO_2, $BiVO_4/TiO_2$ and $BiVO_4/(TiO_2/GO)_{mix}$ at dark and light conditions.

4.1.8 Electrochemical impedance spectroscopy analysis

Electrochemical impedance spectroscopy (EIS) analysis was performed to investigate the kinetics of the charge transfer process of $BiVO_4/(TiO_2/GO)_{mix}$, $BiVO_4/TiO_2$, $BiVO_4$ and TiO_2 photoanodes and the tests were carried out in a 0.1 M Na_2SO_4 solution at the bias potential of 1 V. It is well known that the charge transfer resistance decreases as the arc radius of the EIS plots decreases [70].

As can be observed from Figure 4.10 (a) and (b), the impedance spectra showed a straight line at low frequencies and a semicircle at high frequencies. As shown in Figure 4.10 (a), in comparison to $BiVO_4/(TiO_2/GO)_{mix}$, $BiVO_4/TiO_2$ and $BiVO_4$ samples, the TiO_2 sample displayed the highest impedance arc radius, which indicated a very low efficiency of charge transfer. The semicircle of $BiVO_4$ is smaller than that of TiO_2, which shows better charge transfer characteristics. The lowest arc radius for $BiVO_4/TiO_2$ indicates that the charge transfer and photocatalytic ability of photoanodes were improved by forming the heterojunction. Note that the arc radius of $BiVO_4/(TiO_2/GO)_{mix}$ ternary composite photoanodes is larger than that of $BiVO_4$

and $BiVO_4/TiO_2$. This result is in good agreement with the outcomes of the IPCE, LSV and photocurrent analysis but is inconsistent with previous study [71]. Hence, it could conceivably be hypothesised that part of the photogenerated electrons may react with the OMPs compounds directly or indirectly on the photoanode surface instead of being transferred to the cathode and forming the photocurrent. The reaction mechanism will be discussed in more detail in Section 4.6.

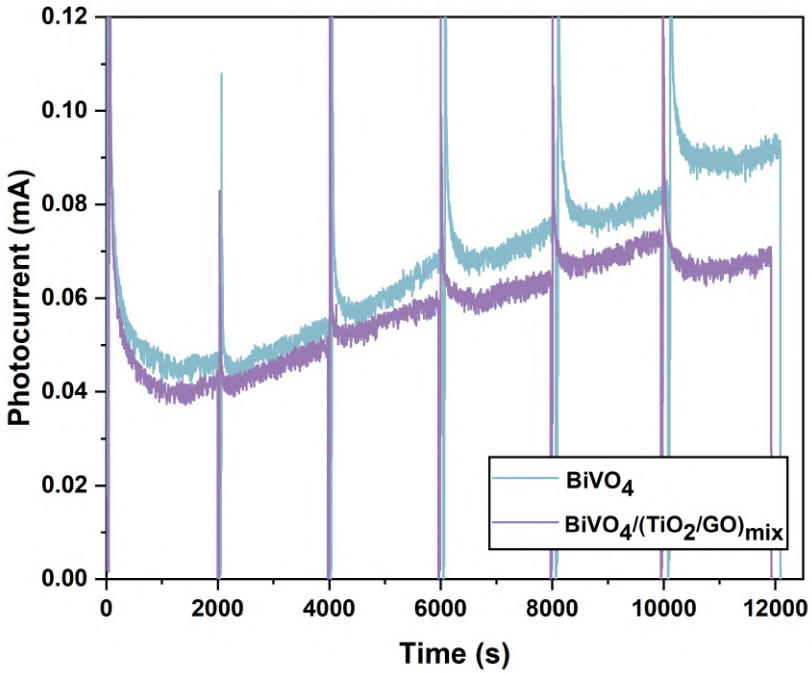

Figure 4.9: Photocurrent versus time plots of $BiVO_4$ and $BiVO_4/(TiO_2/GO)_{mix}$ during degradation experiments

EIS tests of $BiVO_4/(TiO_2/GO)_{mix}$ were also conducted both under illumination and dark conditions as shown in Figure 4.10 (b). It can be seen that the arc radius of the EIS plot under illumination is smaller than that of the EIS plot in dark, which shows that the efficiency of charge transfer is higher and the photoelectrocatalytic ability is more active under illumination condition.

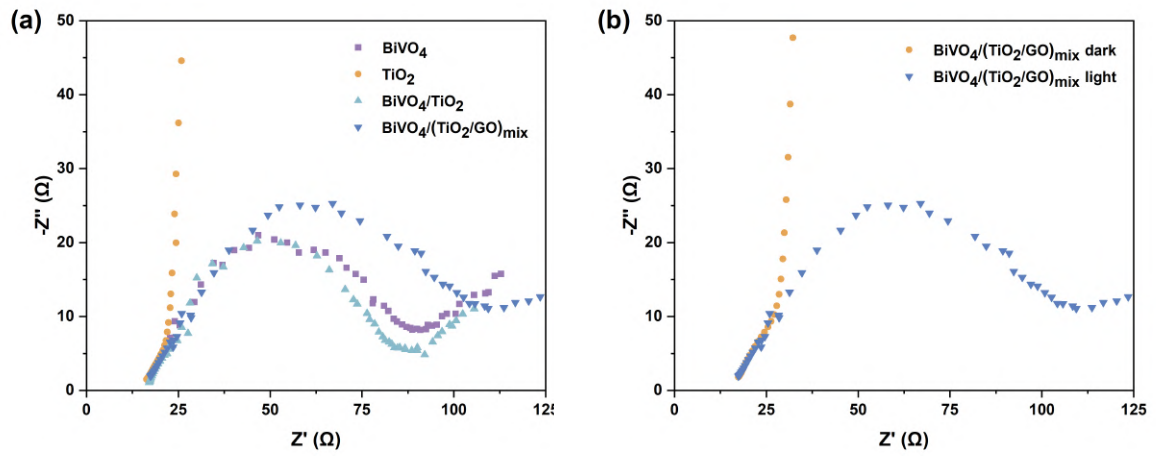

Figure 4.10: EIS plots of (a) $BiVO_4$, TiO_2, $BiVO_4/TiO_2$ and $BiVO_4/(TiO_2/GO)_{mix}$ at light condition, (b) $BiVO_4/(TiO_2/GO)_{mix}$ at dark and light conditions.

4.2 Results of Stage I: Pre-experiments

To evaluate the photoelectrocatalytic degradation capability of the photoanodes and determine the optimal photoanode type used in the OMPs degradation experiments, a typical organic pollutant, methylene blue (MB), was chosen as the indicator pollutant, and the experiment of MB degradation with the concentration of 2.5 $mg \cdot L^{-1}$ was performed in the pre-experiments stage. The photoelectrocatalytic degradation process was performed at a bias potential of 1 V and with 0.1 M Na_2SO_4 as the electrolyte. The irradiance intensity is 60 W/m^2.

As shown in Figure 4.11 (a), the six photoanodes listed in Table 3.2 were used to perform degradation experiments on MB in the conditions described above, photolysis was also included as a blank experiment. The photolysis degradation efficiency of MB was the lowest without the addition of photoanodes, reaching only about 30.71 % after 60 minutes. After 60 min irradiation, bare $BiVO_4$ exhibited only 43.43 % degradation of MB while bare TiO_2 showed 47.84 % MB degradation. After $BiVO_4$ and TiO_2 formed a $BiVO_4/TiO_2$ binary composite heterojunction structure, its degradation efficiency of MB increased to 49.42 % at the same reaction conditions and time. When GO was mixed with TiO_2, the degradation efficiency of the obtained $(TiO_2/GO)_{mix}$ sample for MB increased to 51.97 %. Furthermore, to determine the best layer arrangement of the ternary composite photoanodes, the MB degradation performance of two arrangements: $BiVO_4/(TiO_2/GO)_{mix}$ and $(TiO_2/GO)_{mix}/BiVO_4$ were investigated and com-

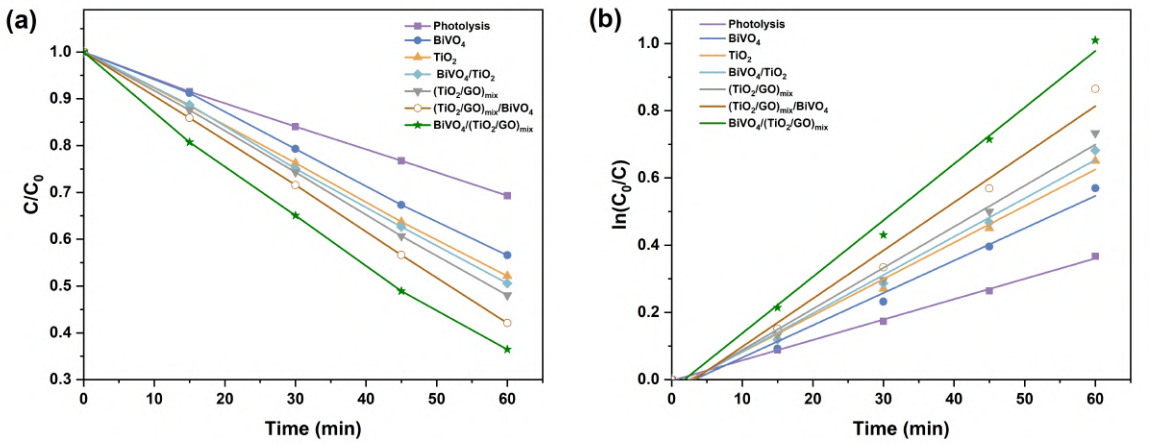

Figure 4.11: (a) Photoelectrocatalytic activity of $BiVO_4$, TiO_2, $BiVO_4/TiO_2$, $(TiO_2/GO)_{mix}$, $BiVO_4/(TiO_2/GO)_{mix}$ and $(TiO_2/GO)_{mix}/BiVO_4$ for degradation of MB, (b) $In(C_0/C)$ plots vs time.

pared. The results exhibited that when $BiVO_4$ thin film is deposited underneath TiO_2 layer, $BiVO_4/(TiO_2/GO)_{mix}$ showed the maximal MB degradation efficiency among all types of photoanodes (63.56 %), while the MB degradation rate of $(TiO_2/GO)_{mix}/BiVO_4$ with the opposite arrangement was slightly lower at 57.90 %. The MB degradation efficiency order was as following: photolysis < $BiVO_4$ < TiO_2 < $BiVO_4/TiO_2$ < $(TiO_2/GO)_{mix}$ < $(TiO_2/GO)_{mix}/BiVO_4$ < $BiVO_4/(TiO_2/GO)_{mix}$.

Table 4.1: Degradation efficiency and kinetics parameters of the as-prepared samples to MB

Photoanodes	**Degradation efficiency (%)**	**k** (min^{-1})	$\mathbf{R^2}$
Photolysis	30.7087	0.0061	0.9988
$BiVO_4$	43.4263	0.0096	0.9874
TiO_2	47.8431	0.0109	0.9907
$BiVO_4/TiO_2$	49.4163	0.0114	0.9899
$(TiO_2/GO)_{mix}$	51.9669	0.0122	0.9878
$(TiO_2/GO)_{mix}/BiVO_4$	57.9060	0.0143	0.9821
$BiVO_4/(TiO_2/GO)_{mix}$	63.5593	0.0168	0.9937

As shown in Figure 4.11 (b), the photoelectrocatalytic degradation reactions of MB fit the first-order kinetic model well. The reaction rate coefficient (k) of photolysis, $BiVO_4$, TiO_2, $BiVO_4/TiO_2$, $(TiO_2/GO)_{mix}$, $(TiO_2/GO)_{mix}/BiVO_4$ and $BiVO_4/(TiO_2/GO)_{mix}$ were 0.0061, 0.0096, 0.0109, 0.0114, 0.0122, 0.0143 and 0.0168 min^{-1}, respectively (Table 4.1). The re-

sults demonstrated that the maximum photoelectrocatalytic activity was obtained from the $BiVO_4/(TiO_2/GO)_{mix}$ ternary composite photoanodes, which was caused by the coupling effect of $BiVO_4$, TiO_2, and GO. Therefore, the $BiVO_4/(TiO_2/GO)_{mix}$ ternary composite photoanodes were used as the optimal photoanodes for the OMPs degradation experiments.

4.3 Results of Stage II: Initial Concentration Experiments

To determine the effect of the initial OMPs concentration on the degradation efficiency of the target OMPs, the stock solutions were diluted to three selected concentrations of 10, 20, and 40 $\mu g{\cdot}L^{-1}$ for the degradation experiments, and all the experiments in this stage were performed with 180 minutes reaction time and neutral initial pH.

The photoelectrocatalytic degradation of the five target OMPs at these three initial concentrations using $BiVO_4/(TiO_2/GO)_{mix}$ photoanodes is shown in Figure 4.12. The degradation efficiencies of DIC were relatively close at all three initial concentrations, with approximately 100 % degradation after 150 minutes (Figure4.12 (a)). The situation was similar for KET, which was almost completely removed after 80 minutes of irradiation (Figure4.12 (b)). As for BTA, the results exhibited that increasing concentration from 10 to 40 $\mu g{\cdot}L^{-1}$ in 180 minutes decreased its degradation efficiency from 29.36 to 19.53 %, respectively (Figure4.12 (c)). One possible reason might be that with higher concentrations of BTA, competition for connector access on the photoanode surface will increase, which leads to a decrease in the removal rate [72]. Also, the higher concentrations of BTA might absorb the incident light and reduce the removal efficiency [73]. However, for CBZ and CAF, the difference between the three initial concentrations was very close, with final degradation rates around 26 % and 9 % after 180 minutes of reaction time, respectively (Figure4.12 (d) and (e)).

Finally, it can be concluded that the difference in initial concentrations did not have any strong effect on the degradation efficiency of the other four target OMPs, except for BTA. Therefore, 10 $\mu g{\cdot}L^{-1}$ was selected as the optimal initial concentration in the subsequent research stages due to the fact that this concentration is more commonly detected in the effluent of WWTPs [20, 74].

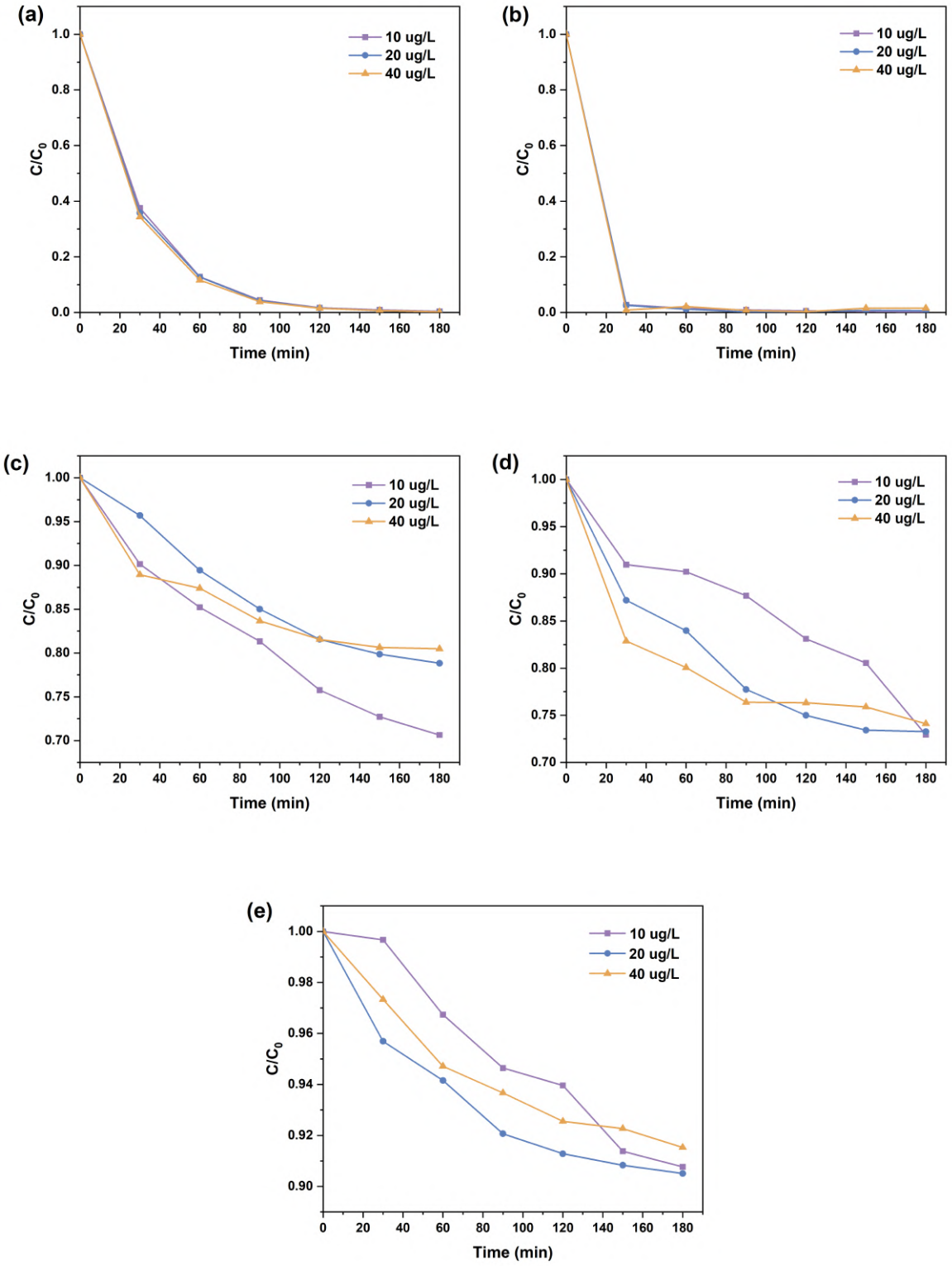

Figure 4.12: Normalized concentration decay versus time plots with initial concentration of 10, 20 and 40 $\mu g{\cdot}L^{-1}$ for (a) DIC, (b) KET, (c) BTA, (d) CBZ and (e) CAF.

4.4 Results of Stage III: Initial pH Experiments

The effect of the initial pH of the OMPs solution on target OMPs degradation efficiency in the range of 3.4-4.0, 6.5-7.0, and 8.5-9.0 was studied in this stage. The conditions of the initial OMPs concentration of 10 $\mu g \cdot L^{-1}$ and reaction time of 180 minutes were kept the same for the degradation experiments with different initial pH.

As shown in Figure 4.13 (a), with the solution's initial pH of 3.5-4.0, DIC was degraded fastest and was removed entirely after about 90 minutes of illumination. However, photoelectrocatalytic degradation was slower at the initial pH range of 6.5-7.0 and 8.5-9.0, both of which achieved 100 % degradation after approximately 150 minutes. For KET, its degradation efficiency was very close for the three initial pH ranges, and all were completely degraded after about 100 minutes (Figure4.13 (b)), indicating that it was not affected by the initial pH change, which is consistent with the results of a previous study [75]. As can be seen in Figure4.13 (c) and (d), the degradation behaviour of BTA and CBZ are very similar as their degradation efficiency increased with the decrease of the initial pH value and can finally reach 35.50 % and 54.07 %, respectively. CAF achieved degradation efficiencies of 33.37 %, 10.69 % and 16.39 % at initial pH in the range of 3.5-4.0, 6.5-7.0 and 8.5-9.0, respectively (Figure4.13 (e)).

It is well known that pH can affect the charge carried by a compound; when the pH value is higher than its pK_a value, the compound is negatively charged and, conversely, when the pH value is lower than its pK_a value, the compound is positively charged [76]. In the case of DIC, its pKa value is 4.13, so it is positively charged at the pH range of 3.5-4.0 $<$ pK_a and negatively charged at the pH range of 6.5-7.0 and 8.5-9.0 $>$ pK_a [77]. In the system in this study, a bias voltage of 1 V is continuously applied between the photoanode and the carbon stick cathode during the degradation experiments, the surface of the photoanode is always positively charged. Therefore, when the pH is around 4, the photoanode and DIC repel each other with the same charge, while when the pH is about 7 and 9, they attract each other with opposite charges. However, this theory is contrary to the results of the degradation experiments which indicates that electrostatic interaction is not the dominant factor for the change in DIC degradation behaviour with pH change. As for BTA, its pK_a is 8.6, so it exists mainly in molecular form in the selected initial pH ranges [78], while the pK_a of CBZ is 2.3 and 13.9, between which it exists in zwitterion forms without any charge, so the degradation behaviours of these two OMPs are

again independent of electrostatic adsorption interactions [79]. Moreover, the pK_a of CAF is 8.3, so it is uncharged at pH 4, and 7 and negatively charged at pH 9. This is inconsistent with the results of its degradation experiments, which further indicates that the degradation efficiencies of target OMPs at different initial pHs are influenced by non-electrostatic interaction factors [80].

Hence, it could conceivably be hypothesised that the decrease of the initial pH (the increase of the H^+ ion concentration) promotes the generation of certain free radicals, thus increasing the degradation efficiency of OMPs [81]. The degradation mechanism and the radicals involved will be discussed in detail in stage V. Finally, 3.5-4.0 was applied as the optimal initial pH range in the subsequent research stages of this study.

4.5 Results of Stage IV: Triplicate & Single OMP Degradation Experiments

Many studies have shown that the high degradation efficiency of certain OMPs can also be achieved by only direct photolysis without addition of any photocatalyst [2, 82]. In addition, previous research also established that bare $BiVO_4$ also showed a good removal performance on some OMPs under simulated solar light [83]. To further prove the superiority of photoelectrocatalysis in the removal of OMPs and the improvement of the ternary composite heterojunction structure on the degradation efficiency of OMPs, degradation experiments of five target OMPs at the initial concentration of 10 $\mu g{\cdot}L^{-1}$ were carried out at the initial pH of 3.5-4.0 using photolysis, $BiVO_4$ and $BiVO_4/(TiO_2/GO)_{mix}$ photoanodes.

As shown in Figure 4.14 (a), DIC was degraded fastest using $BiVO_4/(TiO_2/GO)_{mix}$ ternary composite photoanodes and was completely removed after about 90 minutes. The degradation results of KET are shown in Figure 4.14 (b). Its degradation efficiencies in all three conditions were very close, and all of them reached about 100 % after 60 minutes, which indicates that KET is very sensitive to light and can be completely degraded under direct irradiation [84]. Therefore, its degradation behaviour under PEC is not representative. Furthermore, the degradation behaviours of BTA, CBZ and CAF showed the same trend and the degradation efficiency orders were as following: photolysis $<$ $BiVO_4$ $<$ $BiVO_4/(TiO_2/GO)_{mix}$. Specifically, BAT achieved degradation efficiencies of 35.50 %, 28.25 % and 23.43 % by $BiVO_4/(TiO_2/GO)_{mix}$, $BiVO_4$

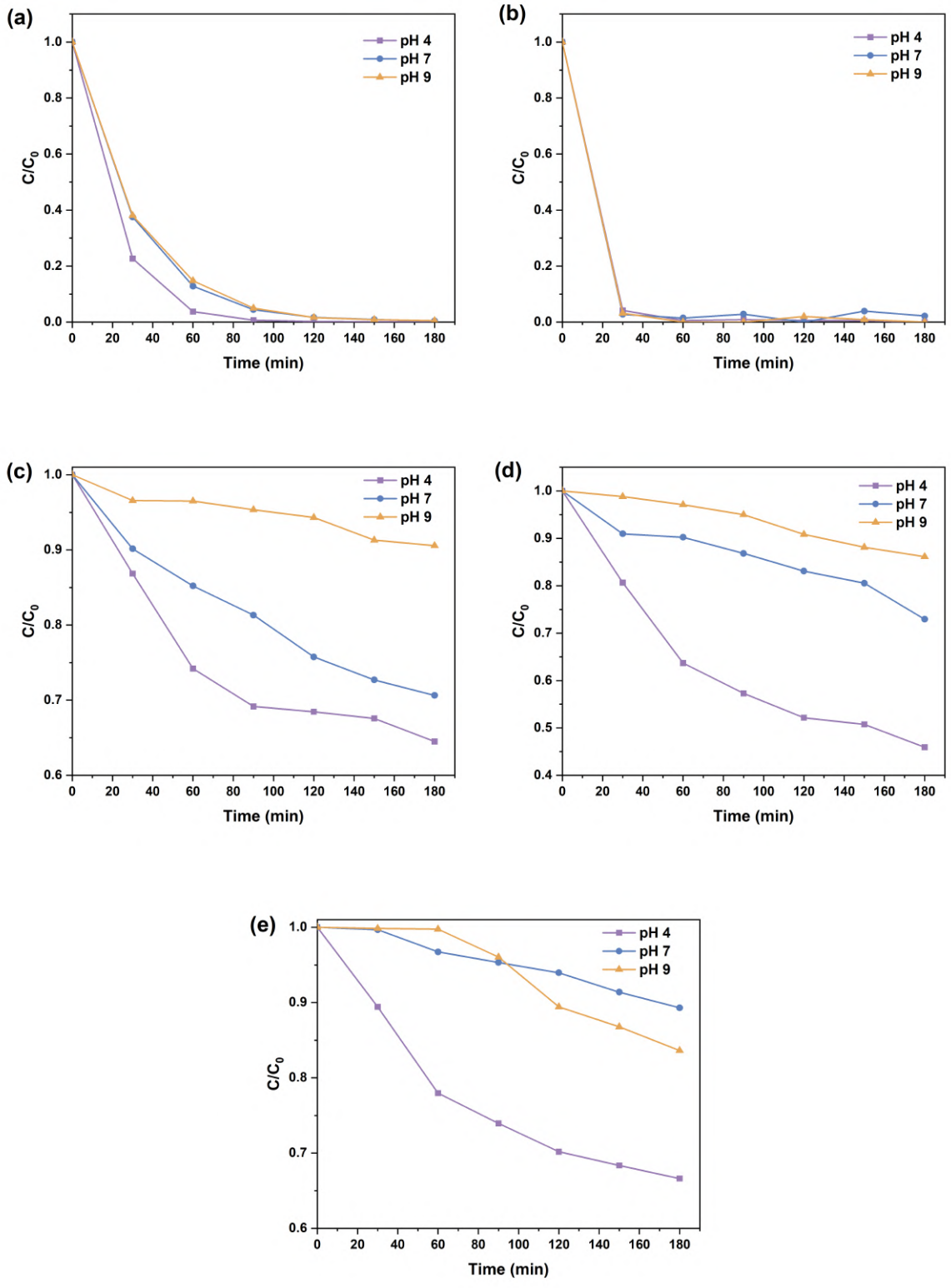

Figure 4.13: Normalized concentration decay versus time plots with initial concentration of 10 $\mu g{\cdot}L^{-1}$ and initial pH of 3.5-4.0, 6.5-7.0 and 8.5-9.0 for (a) DIC, (b) KET, (c) BTA, (d) CBZ and (e) CAF.

and $BiVO_4/(TiO_2/GO)_{mix}$, respectively, while CBZ reached degradation efficiency of 54.07 %, 39.33 % and 23.42 %, respectively. Degradation efficiencies of 33.37 %, 25.09 % and 18.09 % were completed in 180 minutes by $BiVO_4/(TiO_2/GO)_{mix}$, $BiVO_4$ and $BiVO_4/(TiO_2/GO)_{mix}$, respectively, for CAF remove.These results are in good agreement with the findings of the pre-experiments in Stage I, which further demonstrates that the ternary composite heterojunction structure of $BiVO_4/(TiO_2/GO)_{mix}$ has the best photoelectrocatalytic performance in degrading the target OMPs.

The optimal conditions of the initial OMPs concentration and the initial solution pH range were determined to be 10 $\mu g{\cdot}L^{-1}$ and 3.5-4.0, respectively, in stage II and stage III of this study. In addition, the excellent photoelectrocatalytic performance of the ternary composite photoanodes $BiVO_4/(TiO_2/GO)_{mix}$ was demonstrated by the comparison of the OMPs degradation results with photolysis, $BiVO_4$ and $BiVO_4/(TiO_2/GO)_{mix}$. However, from the degradation data of the five target OMPs in the previous stages, it can be found that different OMPs had different degradation behaviours in the photoelectrocatalytic degradation process, and a significant difference between their degradation efficiencies was achieved after 180 minutes. To further confirm that this phenomenon is not a coincidence, triplicate degradation experiments of the mixture of the five target OMPs were performed under the optimal conditions mentioned above, and the experimental results with standard error are shown in Figure 4.15. What can be clearly seen in Figure 4.15 (a) is that KET degraded the fastest and was almost completely degraded after 60 minutes due to its sensitivity to irradiation, as discussed previously. Secondly, DIC achieved 100 % degradation efficiency after 120 min of light exposure. In addition, the degradation efficiencies of the other three OMPs after 180 minutes of reaction were, from largest to smallest, CBZ (49.75 %), BTA (33.07 %) and CAF (31.07 %). Moreover, the kinetics of the degradation of the target OMPs are revealed in Figure 4.15 (b) and the reaction rate coefficient (k) of 0.0923, 0.0394, 0.0043, 0.0026 and 0.0024 min^{-1} were obtained for KET, DIC, CBZ, BTA, and CAF, respectively as shown in Table 4.2. These results suggest that the degradation processes of different OMPs are significantly different. A possible explanation for these results may be the competition between different OMPs during the photoelectrocatalytic degradation process.

To further prove this hypothesis, single OMP degradation experiments were conducted for each of the four target OMPs (BTA, CBZ, DIC and CAF). The initial concentration of single

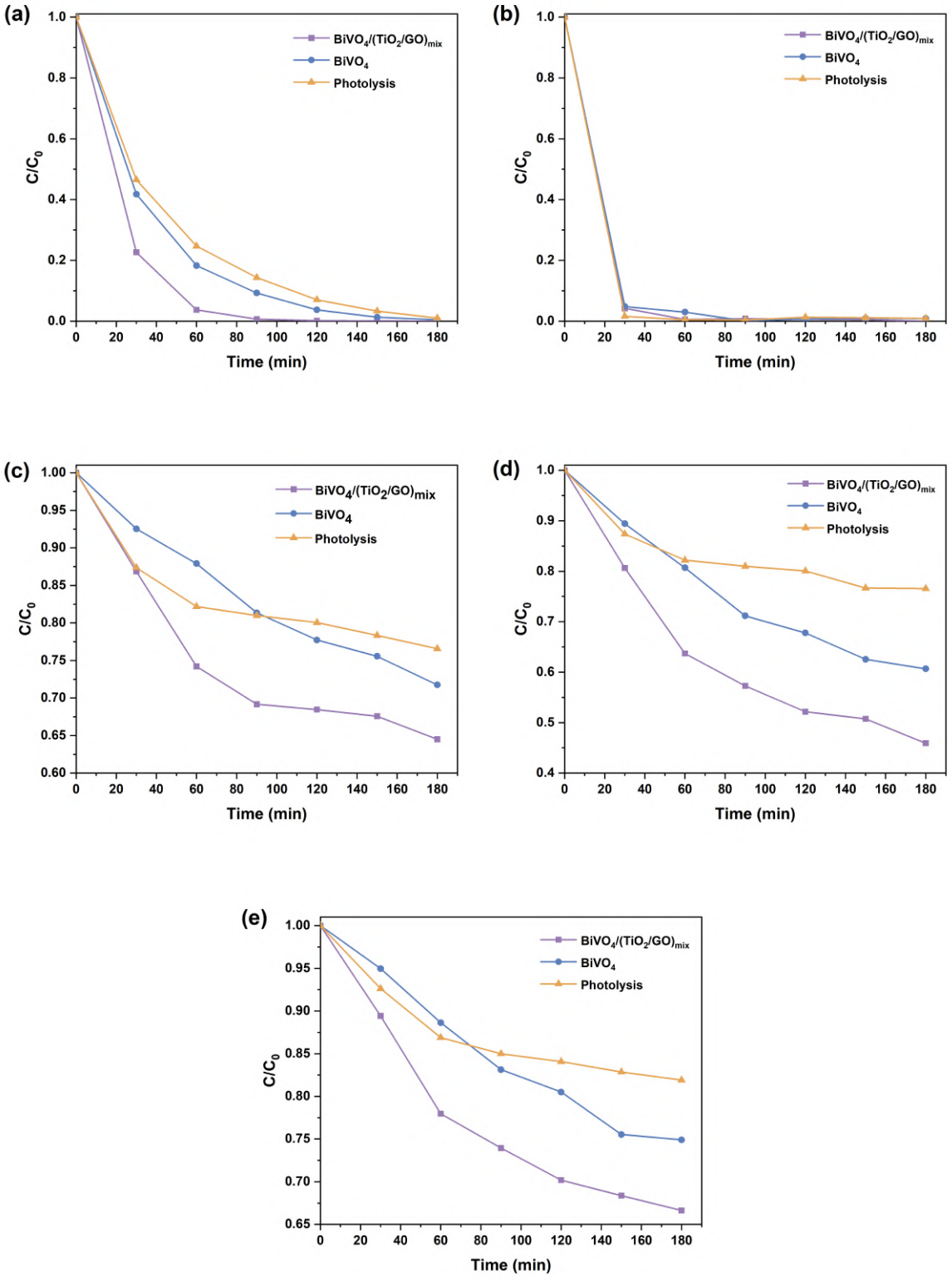

Figure 4.14: Normalized concentration decay versus time plots with $BiVO_4/(TiO_2/GO)_{mix}$, $BiVO_4$ and photolysis for (a) DIC, (b) KET, (c) BTA, (d) CBZ and (e) CAF.

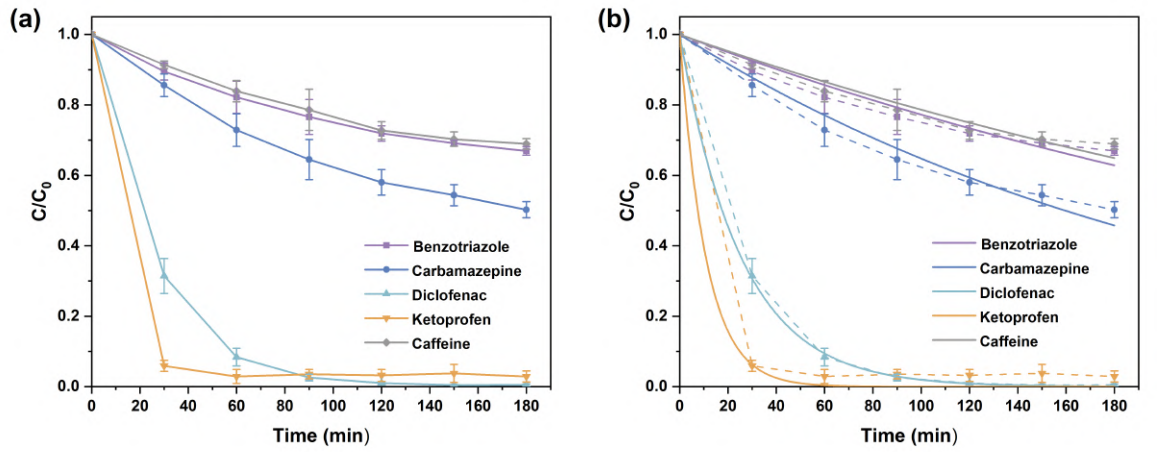

Figure 4.15: (a) Normalized concentration decay versus time plots, (b) Kinetics plots for the degradation of the five target OMPs.

OMP was kept constant at 10 $\mu g{\cdot}L^{-1}$, and the initial pH of the solution was also kept in the range of 3.5-4.0 with the same irradiation time of 180 minutes. The degradation and kinetic results are shown in Figure 4.16, and the specific data are displayed in Table 4.3. It is apparent from the figure that all four OMPs achieved higher degradation efficiency in the single OMP degradation experiments. The reaction rate coefficient (k) of DIC for multiple OMPs and single OMP degradation were 0.0393 and 0.0792 min^{-1}, respectively, which were both the highest among all OMPs, and the difference between the two degradation efficiencies was also the smallest (Figure 4.16 (a) and (b)). Therefore, it could be inferred that DIC would be preferentially degraded in the solution containing the five target OMPs. CAF showed the largest difference between the degradation efficiencies of multiple OMPs and single OMP conditions with 33.37 % and 88.00 %, respectively, an improvement of more than 2.5 times, while reaction rate constants (k) were 0.0024 and 0.01228 min^{-1}, respectively (Figure 4.16 (g) and (h)), which indicates that the competition between multiple OMPs affects CAF's degradation most significantly.

4.6 Results of Stage V: Reusability & Trapping Experiments

To evaluate the reusability and stability of the $BiVO_4/(TiO_2/GO)_{mix}$ ternary composite photoanodes in the long-term degradation process, three cycles of photoelectrocatalytic degradation experiments with the mixture of the five target OMPs using one photoanode (Nine hours in

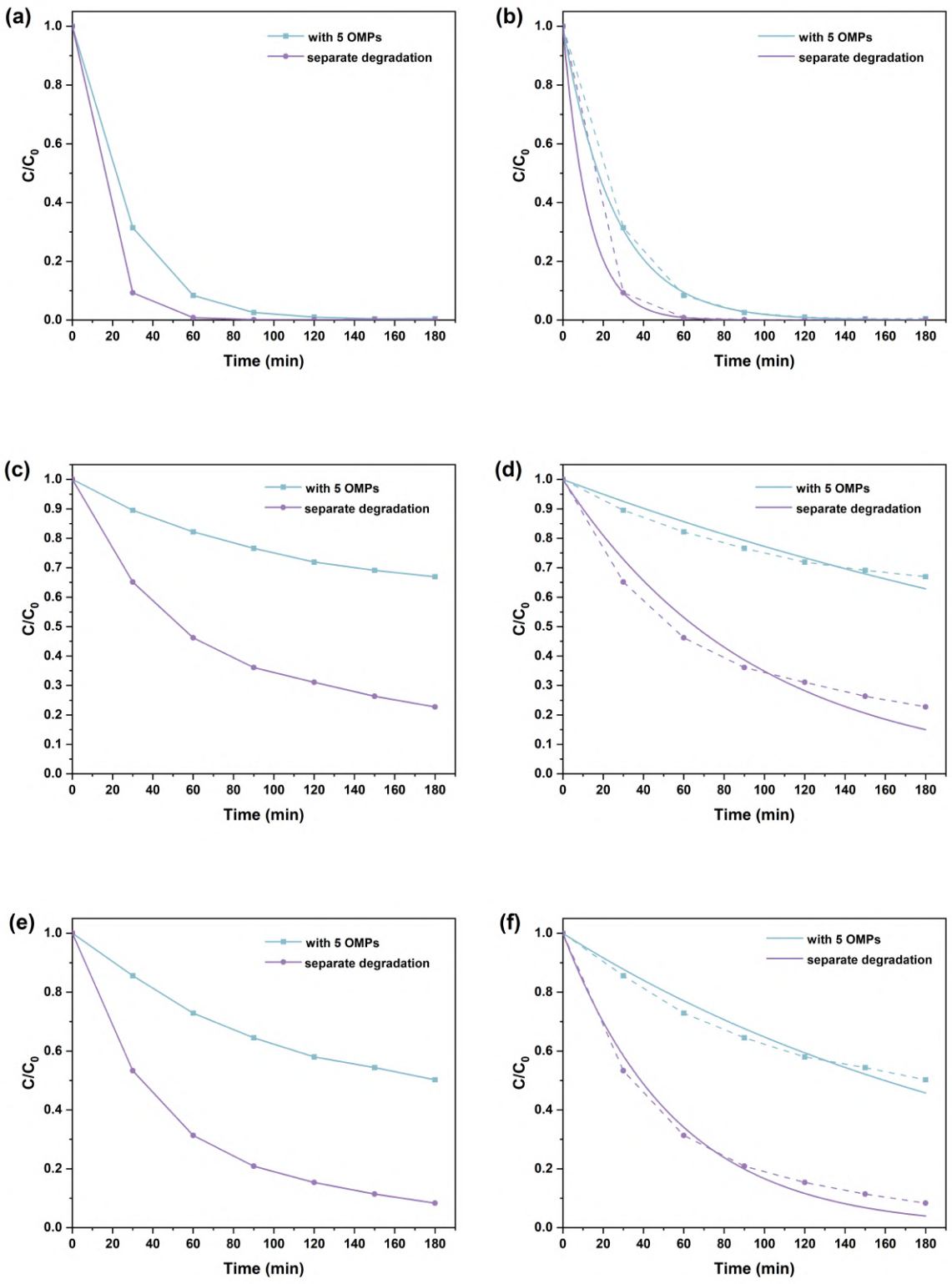
(a)
(b)
(c)
(d)
(e)
(f)
with 5 OMPs
separate degradation
C/C0
Time (min)

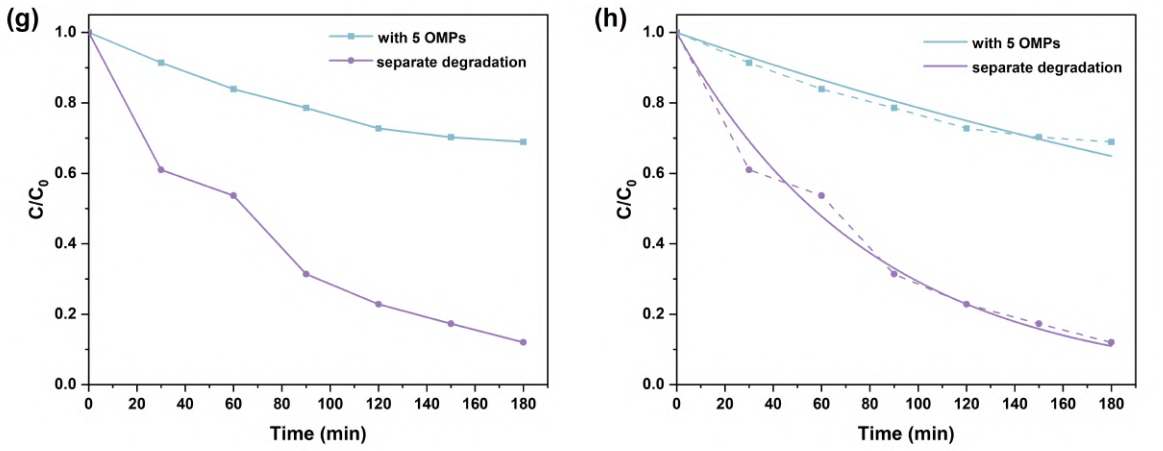

Figure 4.16: Normalized concentration decay versus time plots of single OMP degradation experiments for (a) DIC, (c) BTA, (e) CBZ and (g) CAF; Kinetics plots for the degradation of single OMP degradation experiments for (b) DIC, (d) BTA, (f) CBZ and (h) CAF.

Table 4.2: Degradation efficiency and reaction rate coefficient of the five target OMPs by $BiVO_4/(TiO_2/GO)_{mix}$ photoanodes.

OMPs	**Degradation efficiency (%)**	**k** (min^{-1})	$\mathbf{R^2}$
DIC	99.5200	0.0394	0.9998
KET	97.1070	0.0923	0.9935
BTA	33.0670	0.0026	0.9431
CBZ	49.7530	0.0043	0.9697
CAF	31.0700	0.0024	0.9569

Table 4.3: Degradation efficiency and reaction rate coefficient of single OMP degradation experiments by $BiVO_4/(TiO_2/GO)_{mix}$ photoanodes.

OMPs	**Degradation efficiency (%)**	**k** (min^{-1})	$\mathbf{R^2}$
DIC	99.8909	0.0792	0.9999
BTA	77.2730	0.0105	0.9523
CBZ	91.6814	0.0179	0.9862
CAF	88.0011	0.0123	0.9817

total) were performed. Within each run, $BiVO_4/(TiO_2/GO)_{mix}$ photoanode was exposed to irradiation for 180 minutes before moving from the solution and after each cycle, the electrode was washed using demi water, dried in the air and then reused in the next run. As can be seen from the Figure 4.17, after three cycling runs, the degradation efficiency of the five target OMPs presented no substantial losses, which indicates that the $BiVO_4/(TiO_2/GO)_{mix}$ ternary composite photoanode has good

reusability and stability in the long-term degradation process. Therefore, it is very promising in further applications.

Various active species, including hydroxyl free radicals (·OH), superoxide anions ($O_2^{\cdot -}$), holes (h^+) and electrons (e^-) are induced by the photoanodes during the PEC reaction and it is known that ·OH and $O_2^{\cdot -}$ are the two most efficient active species participating in the OMPs degradation based on previous research [85]. Therefore, for a better understanding of the main reactive species involved in the photoelectrocatalytic degradation process of the target OMPs, trapping experiments were conducted using p-Benzoquinone and methanol as scavengers for the reactive species [52, 86, 87]. For this purpose, 5 mM each of p-Benzoquinone and methanol were added into the OMPs solution before the degradation experiments as scavengers for $O_2^{\cdot -}$ and ·OH, respectively. Figure 4.18 summarizes the results of OMPs degradation with and without these two radical scavengers. It was observed that MeOH did not show a noticeable effect on the degradation of CBZ, DIC and CAF, indicating that ·OH played a minor role in the reaction process. However, the addition of p-Benzoquinone massively decreased the degradation of these three OMPs, suggesting that $O_2^{\cdot -}$ were the most active species in the photoelectrocatalytic process. These results are consistent with previous research which studied the reaction mechanism of CBZ [85], DIC [86] and CAF [87] during photocatalytic degradation process. As for BTA, the degradation efficiency decrease after the addition of methanol was more significant than that after the addition of p-Benzoquinone, which indicates that ·OH played a more important role in the reaction process than $O_2^{\cdot -}$ [52].

The reported mechanism of the photoelectrocatalytic activity of $BiVO_4/TiO_2/GO$ based photocatalyst under UV-visible light can further prove the findings above, according to the equations below [49, 87].

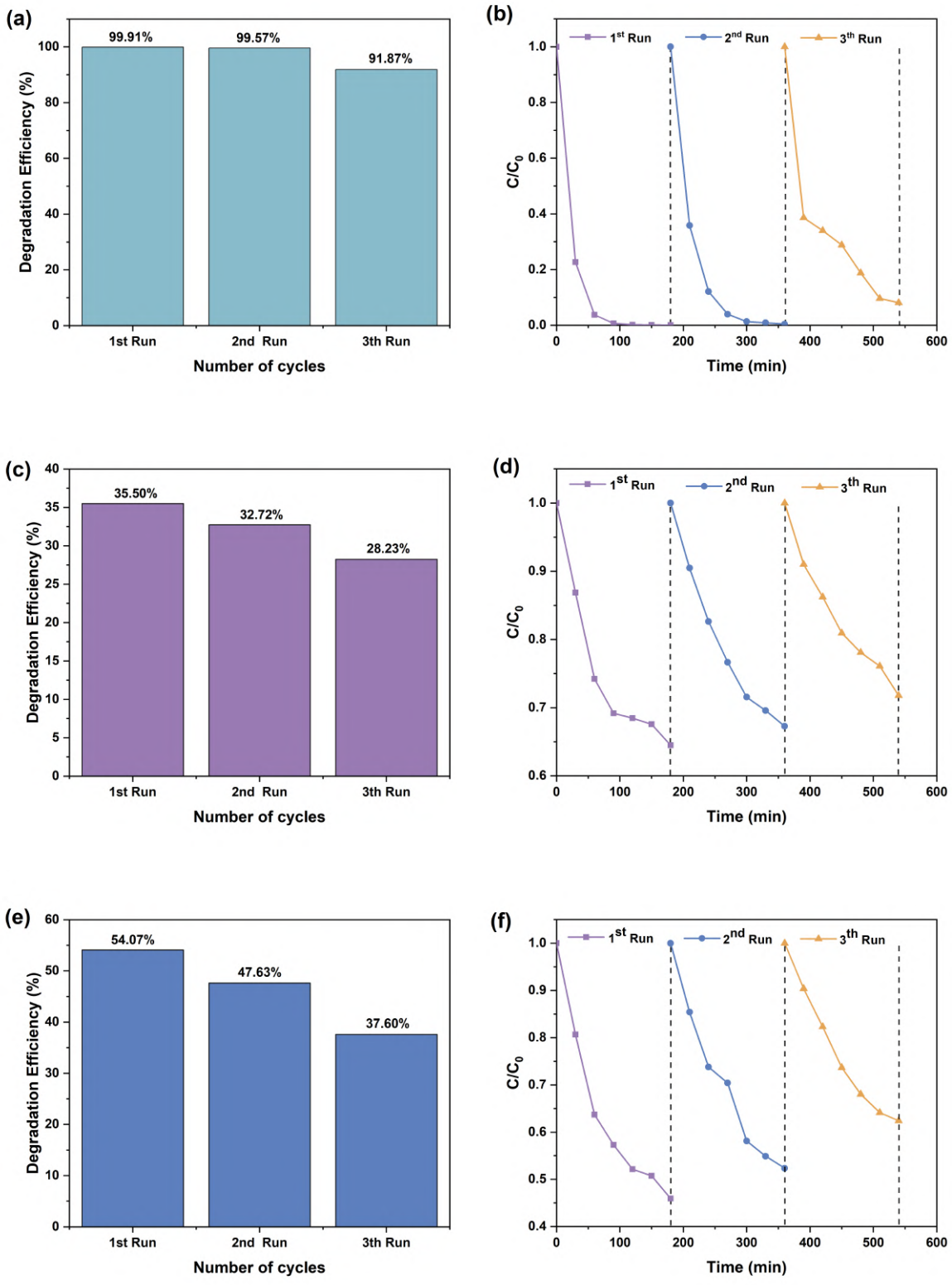
(a)
99.91%
99.57%
91.87%
Degradation Efficiency (%)
1st Run
2nd Run
3th Run
Number of cycles
(b)
1st Run
2nd Run
3th Run
C/C0
Time (min)
(c)
35.50%
32.72%
28.23%
Degradation Efficiency (%)
1st Run
2nd Run
3th Run
Number of cycles
(d)
1st Run
2nd Run
3th Run
C/C0
Time (min)
(e)
54.07%
47.63%
37.60%
Degradation Efficiency (%)
1st Run
2nd Run
3th Run
Number of cycles
(f)
1st Run
2nd Run
3th Run
C/C0
Time (min)

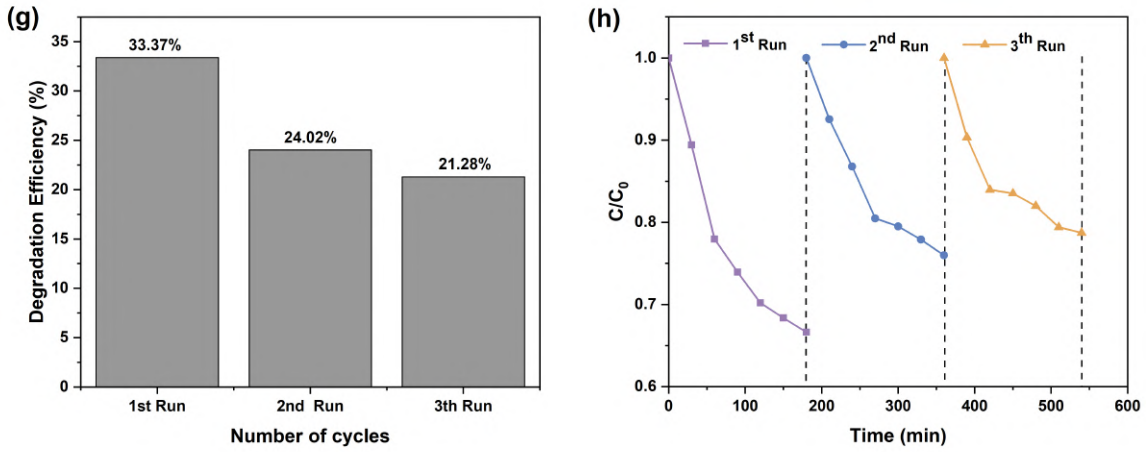

Figure 4.17: Degradation efficiency of recycling experiments for (a) DIC, (c) BTA, (e) CBZ and (g) CAF; Kinetics plots for the degradation of recycling degradation experiments for (b) DIC, (d) BTA, (f) CBZ and (h) CAF.

$$BiVO_4/(TiO_2/GO)_{mix}\ photoanodes \rightarrow h^+ + e^- \tag{2}$$

$$h^+ + e^- \rightarrow Energy \tag{3}$$

$$h^+ + H_2O \rightarrow H^+ + \cdot OH \tag{4}$$

$$h^+ + OH^- \rightarrow \cdot OH \tag{5}$$

$$e^- + O_2 \rightarrow O_2^{\cdot -} \tag{6}$$

$$O_2^{\cdot -} + \cdot OH + OMPs \rightarrow Degradation\ \ byproducts \tag{7}$$

Through the trapping experiments, it is known that $O_2^{\cdot -}$ plays a major role in the degradation of the target OMPs. Therefore, the $O_2^{\cdot -}$ generation reaction in Equation (5) can be inferred as the dominant reaction during the photoelectrocatalytic process. These findings provide further

support for the hypothesis that the separated photogenerated electrons may enter the solution directly to form $O_2^{\cdot -}$ due to the excellent conductivity of GO on the $BiVO_4/(TiO_2/GO)_{mix}$ photoanodes surface, instead of flowing to the cathode to generate photocurrent, as shown in Figure 4.19. This theory may help to explain $BiVO_4/(TiO_2/GO)_{mix}$ photoanode's lower incident photon-to-current efficiency in the IPCE tests (Figure 4.7), its lower current in the LSV tests (Figure 4.8) and lower photocurrent during degradation (Figure 4.9) as well as the larger arc radius of the ternary composite photoanodes in the EIS measurements (Figure 4.10). Due to less photogenerated electrons flowing to the cathode, the measured photocurrent and incident photon-to-current efficiency decreased.

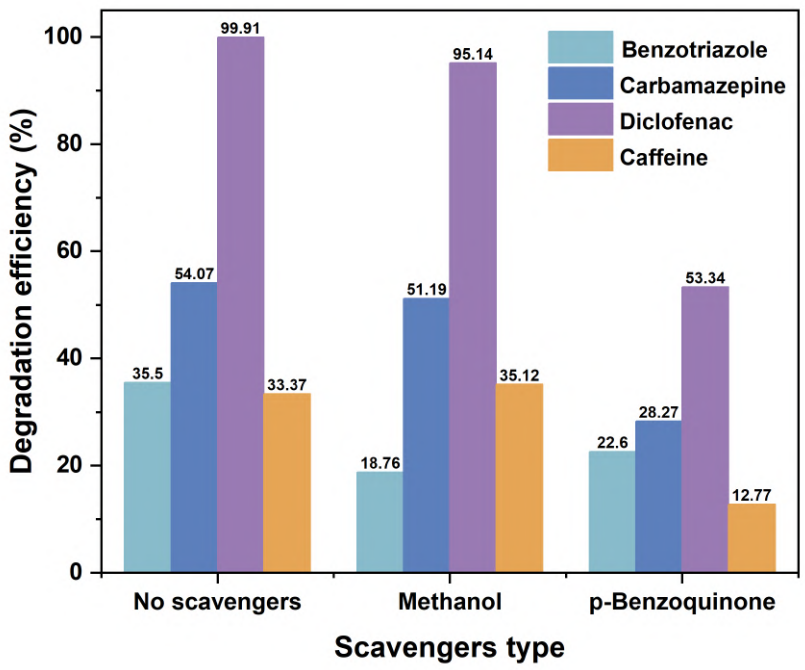

Figure 4.18: Degradation of the five target OMPs in the presence of various scavengers.

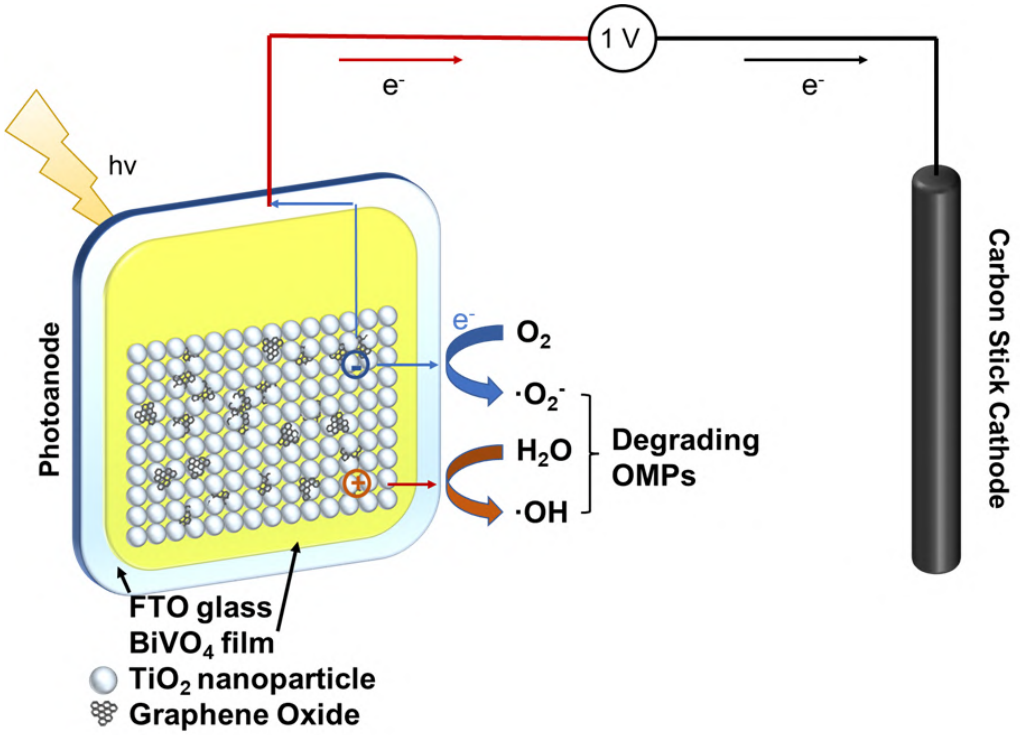

Figure 4.19: Proposed reaction mechanism of $BiVO_4/(TiO_2/GO)_{mix}$ ternary composite photoanodes.

Chapter 5

Conclusions

5.1 Recap of research objective and questions

The objectives of this study was to fabricate ternary composite photoanodes with $BiVO_4$, TiO_2 and GO, and to investigate its photoelectrocatalytic degradation performance and behaviour in an aquatic environment with the five target OMPs and its feasibility in the long-term degradation process. Based on the five stages of experiments, the previous research questions can be answered below:

(1) ***How is the photoelectrocatalytic degradation performance of the $BiVO_4/TiO_2/GO$ ternary composite photoanodes?***

According to the results of pre-experiments of MB degradation and the OMPs degradation experiments using photolysis, $BiVO_4$ and $BiVO_4/(TiO_2/GO)_{mix}$, the $BiVO_4/TiO_2/GO$ ternary composite photoanodes obtained the highest degradation efficiency among all the photoanodes.

(2) ***What is the optimal layer arrangement of the ternary composite photoanodes?***

The results of the pre-experiment indicates that the $BiVO_4/(TiO_2/GO)_{mix}$ ternary composite photoanodes is the optimal photoanode type with $BiVO_4$ layer at the bottom and $(TiO_2/GO)_{mix}$ layer on the top.

(3) ***What are the optimal initial operational conditions on the photoelectrocatalytic degradation process of the five target OMPs using the ternary composite pho-***

toanodes?

- ***What is the optimal initial concentration of target OMPs during the degradation experiments?***

  The result of the experiment in stage II shows that there is no significant difference between the OMPs photoelectrocatalytic degradation performed at the initial concentration of 10, 20 and 40 $\mu g \cdot L^{-1}$. Therefore, 10 $\mu g \cdot L^{-1}$ was selected as the optimal initial concentration in the subsequent research stages because this concentration is more close to the OMPs concentrations detected in the real WWTPs effluent.

- ***What is the optimal initial pH of the target OMPs solution during the degradation experiments?***

  The result of the experiment in stage III shows that the degradation efficiency increased with decreasing initial pH and the highest removal rate was obtained with initial pH in the range of 3.5-4.0.

(4) ***What is the photoelectrocatalytic degradation behaviour of target OMPs in a multiple OMPs environment.***

The competition between different OMPs during the photoelectrocatalytic degradation process was observed in stage IV. DIC was preferentially degraded in the solution containing the five target OMPs, while CAF was affected by the competition most significantly.

(5) ***What is the photoelectrocatalytic degradation performance of the ternary composite photoanodes for the five target OMPs after 2-3 cycles of sequential degradation processes?***

After three cycles of photoelectrocatalytic degradation experiments of OMPs using the same $BiVO_4/(TiO_2/GO)_{mix}$ ternary composite photoanode, the removal efficiency of the five target OMPs presented no obvious losses, which indicates that the ternary composite photoanode has good reusability and stability in the long-term degradation process.

(6) ***What is the reaction mechanism of the photoelectrocatalytic degradation process using the ternary composite photoanodes?***

The result of trapping experiments in stage V showed that $O_2^{\cdot-}$ plays a major role in the degradation of the target OMPs. Therefore, the $O_2^{\cdot-}$ generating reaction via photogenerated electrons were inferred to be the dominant reaction during the photoelectrocatalytic process.

5.2 Overall conclusions

The overall conclusions of this research are as follows:

(1) **Ultrasonic spray pyrolysis has proven to be an effective method for the batch fabrication of thin film photoanodes. $BiVO_4/(TiO_2/GO)_{mix}$ ternary composite photoanodes with superior photoelectrocatalytic properties were obtained by this method.**

(2) **The photoelectrocatalytic degradation of the target OMPs was not significantly influenced by the initial OMPs concentration but was influenced greatly by the initial solution pH, the reason for which is inferred to be related to the effect of non-electrostatic interactions between OMPs molecular and the photoanodes.**

(3) **The $BiVO_4/(TiO_2/GO)_{mix}$ ternary composite photoanode has excellent photoelectrocatalytic performance on the degradation of target OMPs, achieving 31.07 %-99.57% degradation efficiency after 180 minutes of illumination. And it shows good reusability and stability in the long-term degradation process**

(4) **The photocurrent of $BiVO_4/(TiO_2/GO)_{mix}$ ternary composite photoanode was lower than that of bare $BiVO_4$ and $BiVO_4/TiO_2$. The reason might be that the separated photogenerated electrons enter the solution directly to form $O_2^{\cdot-}$ for OMPs degradation due to the excellent conductivity of GO on the ternary composite photoanode surface, instead of flowing to the cathode to generate photocurrent.**

(5) **Different target OMPs had different degradation behaviour, and competition was observed during the photoelectrocatalytic degradation process with multiple OMPs involved.**

(6) **$O_2^{\cdot-}$ were the most active species for target OMPs degradation in the photoelectrocatalytic process of $BiVO_4/(TiO_2/GO)_{mix}$ ternary composite photoanodes.**

Chapter 6

Limitations and Recommendations

6.1 Limitations

Several limitations of this study will be demonstrated in this section.

(1) **Due to the complexity of the real WWTPs effluent, OMPs solution was made for the degradation experiments in this study. Moreover, only five OMPs of concern were selected as target OMPs, while the photoelectrocatalytic degradation of the other OMPs on the watch list by $BiVO_4/(TiO_2/GO)_{mix}$ ternary composite photoanodes was not investigated.**

(2) **The non-electrostatic interactions causing the effect of initial pH on the degradation efficiency of OMPs were not explored in depth.**

(3) **The two target OMPs, KET and DIC, proved to be very sensitive to light, therefore their degradation behaviours are not representative of the PEC degradation.**

(4) **For the three target OMPs, BTA, CBZ and CAF, a degradation time of three hours was shown not sufficient, which might result in an incomplete study of their degradation behaviour.**

(5) **Trapping experiments have demonstrated that $O_2^{\cdot -}$ was the most active species in the degradation process. However, the specific OMPs degradation pathways and reactions have not been investigated.**

6.2 Recommendations

Some suggestions for future research are provided below.

(1) **To investigate the photoelectrocatalytic degradation of OMPs in real WWTPs effluent by $BiVO_4/(TiO_2/GO)_{mix}$ ternary composite photoanodes, further experiments can be conducted using real effluent from local WWTPs.**

(2) **A longer illumination time should be examined to achieve better degradation performance of BTA, CBZ and CAF.**

(3) **Further experiments and analyses of the degradation pathways and by-products generated during the photoelectrocatalytic degradation process are suggested to be conducted to confirm the hypothesis that the separated photogenerated electrons enter the solution directly to form $O_2^{\cdot -}$.**

(4) **To further improve the photoelectrocatalytic performance of the ternary composite photoanodes, the concentration of each material, as well as the ratio, should be investigated, and some promising materials such as reduced graphene oxide (RGO), should be applied in future research.**

Bibliography

[1] B. S. Rathi, P. S. Kumar, and P.-L. Show, "A review on effective removal of emerging contaminants from aquatic systems: current trends and scope for further research," *Journal of Hazardous Materials*, vol. 409, p. 124413, 2021.

[2] W. Yang, H. Zhou, and N. Cicek, "Treatment of organic micropollutants in water and wastewater by uv-based processes: a literature review," *Critical Reviews in Environmental Science and Technology*, vol. 44, no. 13, pp. 1443–1476, 2014.

[3] K. Noguera-Oviedo and D. S. Aga, "Lessons learned from more than two decades of research on emerging contaminants in the environment," *Journal of hazardous materials*, vol. 316, pp. 242–251, 2016.

[4] D. K. Kanaujiya, T. Paul, A. Sinharoy, and K. Pakshirajan, "Biological treatment processes for the removal of organic micropollutants from wastewater: a review," *Current pollution reports*, vol. 5, no. 3, pp. 112–128, 2019.

[5] M. Arslan, I. Ullah, J. A. Müller, N. Shahid, and M. Afzal, "Organic micropollutants in the environment: ecotoxicity potential and methods for remediation," *Enhancing cleanup of environmental pollutants*, pp. 65–99, 2017.

[6] P. Xue, Y. Zhao, D. Zhao, M. Chi, Y. Yin, Y. Xuan, and X. Wang, "Mutagenicity, health risk, and disease burden of exposure to organic micropollutants in water from a drinking water treatment plant in the yangtze river delta, china," *Ecotoxicology and Environmental Safety*, vol. 221, p. 112421, 2021.

[7] Y. Luo, W. Guo, H. H. Ngo, L. D. Nghiem, F. I. Hai, J. Zhang, S. Liang, and X. C. Wang, "A review on the occurrence of micropollutants in the aquatic environment and their

fate and removal during wastewater treatment," *Science of the total environment*, vol. 473, pp. 619–641, 2014.

[8] P. R. Rout, T. C. Zhang, P. Bhunia, and R. Y. Surampalli, "Treatment technologies for emerging contaminants in wastewater treatment plants: A review," *Science of the Total Environment*, vol. 753, p. 141990, 2021.

[9] M. Sackaria and L. Elango, "Organic micropollutants in groundwater of india—a review," *Water Environment Research*, vol. 92, no. 4, pp. 504–523, 2020.

[10] Y. Yu, W. Y. Mo, and T. Luukkonen, "Adsorption behaviour and interaction of organic micropollutants with nano and microplastics–a review," *Science of the Total Environment*, vol. 797, p. 149140, 2021.

[11] K. Gautam and S. Anbumani, "Ecotoxicological effects of organic micro-pollutants on the environment," in *Current developments in biotechnology and bioengineering*, pp. 481–501, Elsevier, 2020.

[12] R. Tröger, S. J. Köhler, V. Franke, O. Bergstedt, and K. Wiberg, "A case study of organic micropollutants in a major swedish water source–removal efficiency in seven drinking water treatment plants and influence of operational age of granulated active carbon filters," *Science of The Total Environment*, vol. 706, p. 135680, 2020.

[13] M. Sörengård, H. Campos-Pereira, M. Ullberg, F. Y. Lai, O. Golovko, and L. Ahrens, "Mass loads, source apportionment, and risk estimation of organic micropollutants from hospital and municipal wastewater in recipient catchments," *Chemosphere*, vol. 234, pp. 931–941, 2019.

[14] J. Sánchez-Avila, R. Tauler, and S. Lacorte, "Organic micropollutants in coastal waters from nw mediterranean sea: sources distribution and potential risk," *Environment International*, vol. 46, pp. 50–62, 2012.

[15] M. A. Launay, U. Dittmer, and H. Steinmetz, "Organic micropollutants discharged by combined sewer overflows–characterisation of pollutant sources and stormwater-related processes," *Water Research*, vol. 104, pp. 82–92, 2016.

[16] R. D. Turner, M. S. J. Warne, L. A. Dawes, K. Thompson, and G. D. Will, "Greywater irrigation as a source of organic micro-pollutants to shallow groundwater and nearby surface water," *Science of the Total Environment*, vol. 669, pp. 570–578, 2019.

[17] M. O. Barbosa, N. F. Moreira, A. R. Ribeiro, M. F. Pereira, and A. M. Silva, "Occurrence and removal of organic micropollutants: An overview of the watch list of eu decision 2015/495," *Water research*, vol. 94, pp. 257–279, 2016.

[18] B. Kasprzyk-Hordern, R. M. Dinsdale, and A. J. Guwy, "The removal of pharmaceuticals, personal care products, endocrine disruptors and illicit drugs during wastewater treatment and its impact on the quality of receiving waters," *Water research*, vol. 43, no. 2, pp. 363–380, 2009.

[19] S. K. Maeng, B. G. Choi, K. T. Lee, and K. G. Song, "Influences of solid retention time, nitrification and microbial activity on the attenuation of pharmaceuticals and estrogens in membrane bioreactors," *Water research*, vol. 47, no. 9, pp. 3151–3162, 2013.

[20] R. Guillossou, J. Le Roux, R. Mailler, E. Vulliet, C. Morlay, F. Nauleau, J. Gasperi, and V. Rocher, "Organic micropollutants in a large wastewater treatment plant: what are the benefits of an advanced treatment by activated carbon adsorption in comparison to conventional treatment?," *Chemosphere*, vol. 218, pp. 1050–1060, 2019.

[21] N. K. Khanzada, M. U. Farid, J. A. Kharraz, J. Choi, C. Y. Tang, L. D. Nghiem, A. Jang, and A. K. An, "Removal of organic micropollutants using advanced membrane-based water and wastewater treatment: A review," *Journal of membrane science*, vol. 598, p. 117672, 2020.

[22] R. Dewil, D. Mantzavinos, I. Poulios, and M. A. Rodrigo, "New perspectives for advanced oxidation processes," *Journal of environmental management*, vol. 195, pp. 93–99, 2017.

[23] D. B. Miklos, C. Remy, M. Jekel, K. G. Linden, J. E. Drewes, and U. Hübner, "Evaluation of advanced oxidation processes for water and wastewater treatment–a critical review," *Water Research*, vol. 139, pp. 118–131, 2018.

[24] L. L. Silva, C. G. Moreira, B. A. Curzio, F. V. da Fonseca, *et al.*, "Micropollutant removal

from water by membrane and advanced oxidation processes—a review," *Journal of Water Resource and Protection*, vol. 9, no. 05, p. 411, 2017.

[25] N. F. Moreira, C. Narciso-da Rocha, M. I. Polo-López, L. M. Pastrana-Martínez, J. L. Faria, C. M. Manaia, P. Fernandez-Ibanez, O. C. Nunes, and A. M. Silva, "Solar treatment (h2o2, tio2-p25 and go-tio2 photocatalysis, photo-fenton) of organic micropollutants, human pathogen indicators, antibiotic resistant bacteria and related genes in urban wastewater," *Water research*, vol. 135, pp. 195–206, 2018.

[26] S. N. Frank and A. J. Bard, "Heterogeneous photocatalytic oxidation of cyanide ion in aqueous solutions at titanium dioxide powder," *Journal of the American Chemical Society*, vol. 99, no. 1, pp. 303–304, 1977.

[27] S. Gu, W. Li, F. Wang, S. Wang, H. Zhou, and H. Li, "Synthesis of buckhorn-like bivo4 with a shell of ceox nanodots: Effect of heterojunction structure on the enhancement of photocatalytic activity," *Applied Catalysis B: Environmental*, vol. 170, pp. 186–194, 2015.

[28] J.-q. Li, Z.-w. Zhou, X. Li, Y.-l. Yang, J.-f. Gao, R. Yu, H.-p. Wang, and N. Wang, "Synergistically boosting sulfamerazine degradation via activation of peroxydisulfate by photocatalysis of bi2o3-tio2/pac under visible light irradiation," *Chemical Engineering Journal*, vol. 428, p. 132613, 2022.

[29] J. S. Chang, Y. W. Phuan, M. N. Chong, and J. D. Ocon, "Exploration of a novel type ii 1d-zno nanorods/bivo4 heterojunction photocatalyst for water depollution," *Journal of Industrial and Engineering Chemistry*, vol. 83, pp. 303–314, 2020.

[30] P. Fernandez-Ibanez, S. McMichael, A. R. Cabanillas, S. Alkharabsheh, A. T. Moranchel, and J. A. Byrne, "New trends on photoelectrocatalysis (pec): nanomaterials, wastewater treatment and hydrogen generation," *Current Opinion in Chemical Engineering*, vol. 34, p. 100725, 2021.

[31] S. McMichael, P. Fernández-Ibáñez, and J. A. Byrne, "A review of photoelectrocatalytic reactors for water and wastewater treatment," *Water*, vol. 13, no. 9, p. 1198, 2021.

[32] S. Garcia-Segura and E. Brillas, "Applied photoelectrocatalysis on the degradation of organic

pollutants in wastewaters," *Journal of Photochemistry and Photobiology C: Photochemistry Reviews*, vol. 31, pp. 1–35, 2017.

[33] D. Cao, Y. Wang, and X. Zhao, "Combination of photocatalytic and electrochemical degradation of organic pollutants from water," *Current Opinion in Green and Sustainable Chemistry*, vol. 6, pp. 78–84, 2017.

[34] M. F. R. Samsudin, R. Bashiri, N. M. Mohamed, Y. H. Ng, and S. Sufian, "Tailoring the morphological structure of bivo4 photocatalyst for enhanced photoelectrochemical solar hydrogen production from natural lake water," *Applied Surface Science*, vol. 504, p. 144417, 2020.

[35] Y. Zhang, X. Xiong, Y. Han, X. Zhang, F. Shen, S. Deng, H. Xiao, X. Yang, G. Yang, and H. Peng, "Photoelectrocatalytic degradation of recalcitrant organic pollutants using tio2 film electrodes: an overview," *Chemosphere*, vol. 88, no. 2, pp. 145–154, 2012.

[36] Y. Zhou, X. Fan, G. Zhang, and W. Dong, "Fabricating mos2 nanoflakes photoanode with unprecedented high photoelectrochemical performance and multi-pollutants degradation test for water treatment," *Chemical Engineering Journal*, vol. 356, pp. 1003–1013, 2019.

[37] M. G. Peleyeju and E. L. Viljoen, "Wo3-based catalysts for photocatalytic and photoelectrocatalytic removal of organic pollutants from water–a review," *Journal of Water Process Engineering*, vol. 40, p. 101930, 2021.

[38] W. Sang, G. Zhang, H. Lan, X. An, and H. Liu, "The effect of different exposed facets on the photoelectrocatalytic degradation of o-chlorophenol using p-type cu2o crystals," *Electrochimica Acta*, vol. 231, pp. 429–436, 2017.

[39] C. J. Lin, S.-J. Liao, L.-C. Kao, and S. Y. H. Liou, "Photoelectrocatalytic activity of a hydrothermally grown branched zno nanorod-array electrode for paracetamol degradation," *Journal of hazardous materials*, vol. 291, pp. 9–17, 2015.

[40] Y. Li, X. Sun, Y. Tang, Y. H. Ng, L. Li, F. Jiang, J. Wang, W. Chen, and L. Li, "Understanding photoelectrocatalytic degradation of tetracycline over three-dimensional coral-like zno/bivo4 nanocomposite," *Materials Chemistry and Physics*, vol. 271, p. 124871, 2021.

[41] H. Wu, R. Irani, K. Zhang, L. Jing, H. Dai, H. Y. Chung, F. F. Abdi, and Y. H. Ng, "Unveiling carrier dynamics in periodic porous bivo4 photocatalyst for enhanced solar water splitting," *ACS Energy Letters*, vol. 6, no. 10, pp. 3400–3407, 2021.

[42] W. P. Utomo, M. K. Leung, Z. Yin, H. Wu, and Y. H. Ng, "Advancement of bismuth-based materials for electrocatalytic and photo (electro) catalytic ammonia synthesis," *Advanced Functional Materials*, p. 2106713, 2021.

[43] C. V. Reddy, I. N. Reddy, R. Koutavarapu, K. R. Reddy, D. Kim, and J. Shim, "Novel bivo4 nanostructures for environmental remediation, enhanced photoelectrocatalytic water oxidation and electrochemical energy storage performance," *Solar Energy*, vol. 207, pp. 441–449, 2020.

[44] M. F. R. Samsudin, S. Sufian, and B. Hameed, "Epigrammatic progress and perspective on the photocatalytic properties of bivo4-based photocatalyst in photocatalytic water treatment technology: A review," *Journal of Molecular Liquids*, vol. 268, pp. 438–459, 2018.

[45] N. Kiama and C. Ponchio, "Photoelectrocatalytic performance improvement of bivo4 thin film fabrication via effecting of calcination temperature strategy," *Surface and Coatings Technology*, vol. 383, p. 125257, 2020.

[46] B. O. Orimolade, B. A. Koiki, G. M. Peleyeju, and O. A. Arotiba, "Visible light driven photoelectrocatalysis on a fto/bivo4/bioi anode for water treatment involving emerging pharmaceutical pollutants," *Electrochimica Acta*, vol. 307, pp. 285–292, 2019.

[47] O. Monfort, T. Roch, M. Gregor, L. Satrapinskyy, D. Raptis, P. Lianos, and G. Plesch, "Photooxidative properties of various bivo4/tio2 layered composite films and study of their photocatalytic mechanism in pollutant degradation," *Journal of Environmental Chemical Engineering*, vol. 5, no. 5, pp. 5143–5149, 2017.

[48] X. Shi, I. Y. Choi, K. Zhang, J. Kwon, D. Y. Kim, J. K. Lee, S. H. Oh, J. K. Kim, and J. H. Park, "Efficient photoelectrochemical hydrogen production from bismuth vanadate-decorated tungsten trioxide helix nanostructures," *Nature communications*, vol. 5, no. 1, pp. 1–8, 2014.

[49] Z. Zhu, Q. Han, D. Yu, J. Sun, and B. Liu, "A novel pn heterojunction of bivo4/tio2/go composite for enhanced visible-light-driven photocatalytic activity," *Materials Letters*, vol. 209, pp. 379–383, 2017.

[50] J.-S. Yang, W. W.-P. Lai, S. C. Panchangam, and A. Y.-C. Lin, "Photoelectrochemical degradation of perfluorooctanoic acid (pfoa) with gop25/fto anodes: Intermediates and reaction pathways," *Journal of hazardous materials*, vol. 391, p. 122247, 2020.

[51] N. Lv, Y. Li, Z. Huang, T. Li, S. Ye, D. D. Dionysiou, and X. Song, "Synthesis of go/tio2/bi2wo6 nanocomposites with enhanced visible light photocatalytic degradation of ethylene," *Applied Catalysis B: Environmental*, vol. 246, pp. 303–311, 2019.

[52] J. Xu, L. Li, C. Guo, Y. Zhang, and S. Wang, "Removal of benzotriazole from solution by biobr photocatalysis under simulated solar irradiation," *Chemical Engineering Journal*, vol. 221, pp. 230–237, 2013.

[53] A. S. Mestre and A. P. Carvalho, "Photocatalytic degradation of pharmaceuticals carbamazepine, diclofenac, and sulfamethoxazole by carbon materials: a review," *Molecules*, vol. 24, no. 20, p. 3702, 2019.

[54] A. Smỳkalová, B. Sokolová, K. Foniok, V. Matějka, and P. Praus, "Photocatalytic degradation of selected pharmaceuticals using g-c3n4 and tio2 nanomaterials," *Nanomaterials*, vol. 9, no. 9, p. 1194, 2019.

[55] G. Xu, M. Li, Y. Wang, N. Zheng, L. Yang, H. Yu, and Y. Yu, "A novel ag-biobr-rgo photocatalyst for enhanced ketoprofen degradation: Kinetics and mechanisms," *Science of The Total Environment*, vol. 678, pp. 173–180, 2019.

[56] M. Ghosh, K. Manoli, X. Shen, J. Wang, and A. K. Ray, "Solar photocatalytic degradation of caffeine with titanium dioxide and zinc oxide nanoparticles," *Journal of Photochemistry and Photobiology A: Chemistry*, vol. 377, pp. 1–7, 2019.

[57] E. U. Directive, "39/eu of the european parliament and of the council of 12 august 2013 amending directives 2000/60/ec and 2008/105/ec as regards priority substances in the field of water policy," *Luxembourg: Official Journal of the European Union*, vol. 24, 2013.

[58] K. Zhang, Y. Liu, J. Deng, S. Xie, X. Zhao, J. Yang, Z. Han, and H. Dai, "Co–pd/bivo4: High-performance photocatalysts for the degradation of phenol under visible light irradiation," *Applied Catalysis B: Environmental*, vol. 224, pp. 350–359, 2018.

[59] E. Han, K. Vijayarangamuthu, J.-s. Youn, Y.-K. Park, S.-C. Jung, and K.-J. Jeon, "Degussa p25 tio2 modified with h2o2 under microwave treatment to enhance photocatalytic properties," *Catalysis Today*, vol. 303, pp. 305–312, 2018.

[60] A. Nanakkal and L. Alexander, "Graphene/bivo4/tio2 nanocomposite: tuning band gap energies for superior photocatalytic activity under visible light," *Journal of Materials Science*, vol. 52, no. 13, pp. 7997–8006, 2017.

[61] K. S. Ramaiah and V. S. Raja, "Structural and electrical properties of fluorine doped tin oxide films prepared by spray-pyrolysis technique," *Applied Surface Science*, vol. 253, no. 3, pp. 1451–1458, 2006.

[62] O. A. Krysiak, J. R. Junqueira, F. Conzuelo, T. Bobrowski, J. Masa, A. Wysmolek, and W. Schuhmann, "Importance of catalyst–photoabsorber interface design configuration on the performance of mo-doped bivo4 water splitting photoanodes," *Journal of Solid State Electrochemistry*, vol. 25, no. 1, pp. 173–185, 2021.

[63] E. Aguilera-Ruiz, P. Zambrano-Robledo, J. Vazquez-Arenas, B. Cruz-Ortiz, J. Peral, and U. M. García-Pérez, "Photoactivity of nanostructured spheres of bivo4 synthesized by ultrasonic spray pyrolysis at low temperature," *Materials Research Bulletin*, vol. 143, p. 111447, 2021.

[64] J.-A. Park, B. Yang, J. Lee, I. G. Kim, J.-H. Kim, J.-W. Choi, H.-D. Park, I. W. Nah, and S.-H. Lee, "Ultrasonic spray pyrolysis synthesis of reduced graphene oxide/anatase tio2 composite and its application in the photocatalytic degradation of methylene blue in water," *Chemosphere*, vol. 191, pp. 738–746, 2018.

[65] K. Hu, Y. Li, X. Zhao, D. Zhao, W. Zhao, H. Rong, *et al.*, "Photocatalytic degradation mechanism of the visible-light responsive bivo4/tio2 core–shell heterojunction photocatalyst," *Journal of Inorganic and Organometallic Polymers and Materials*, vol. 30, no. 3, pp. 775–788, 2020.

[66] S. Ullah, A. A. Khan, A. Jan, S. Q. Aain, E. P. Neto, Y. E. Serge-Correales, R. Parveen, H. Wender, U. P. Rodrigues-Filho, S. J. Ribeiro, *et al.*, "Enhanced photoactivity of bivo4/ag/ag2o z-scheme photocatalyst for efficient environmental remediation under natural sunlight and low-cost led illumination," *Colloids and Surfaces A: Physicochemical and Engineering Aspects*, vol. 600, p. 124946, 2020.

[67] X. Yu, Z. Zhao, N. Ren, J. Liu, D. Sun, L. Ding, and H. Liu, "Top or bottom, assembling modules determine the photocatalytic property of the sheetlike nanostructured hybrid photocatalyst composed with sn3o4 and rgo (gqd)," *ACS Sustainable Chemistry & Engineering*, vol. 6, no. 9, pp. 11775–11782, 2018.

[68] A. AlShammari, M. Halim, F. Yam, and N. M. Kaus, "Synthesis of titanium dioxide (tio2)/reduced graphene oxide (rgo) thin film composite by spray pyrolysis technique and its physical properties," *Materials Science in Processing*, vol. 116, p. 105140, 2020.

[69] N. T. T. Tran, S.-Y. Lin, O. E. Glukhova, and M.-F. Lin, "π-bonding-dominated energy gaps in graphene oxide," *RSC advances*, vol. 6, no. 29, pp. 24458–24463, 2016.

[70] D. Hongxing, L. Qiuping, and H. Yuehui, "Preparation of nanoporous bivo4/tio2/ti film through electrodeposition for photoelectrochemical water splitting," *Royal Society open science*, vol. 5, no. 9, p. 180728, 2018.

[71] A. Sadeghzadeh-Attar, "Boosting the photocatalytic ability of hybrid bivo4-tio2 heterostructure nanocomposites for h2 production by reduced graphene oxide (rgo)," *Journal of the Taiwan Institute of Chemical Engineers*, vol. 111, pp. 325–336, 2020.

[72] B. Rahimi and A. Ebrahimi, "Photocatalytic process for total arsenic removal using an innovative bivo4/tio2/led system from aqueous solution: optimization by response surface methodology (rsm)," *Journal of the Taiwan institute of chemical engineers*, vol. 101, pp. 64–79, 2019.

[73] F. Wang, Y. Feng, P. Chen, Y. Wang, Y. Su, Q. Zhang, Y. Zeng, Z. Xie, H. Liu, Y. Liu, *et al.*, "Photocatalytic degradation of fluoroquinolone antibiotics using ordered mesoporous g-c3n4 under simulated sunlight irradiation: kinetics, mechanism, and antibacterial activity elimination," *Applied Catalysis B: Environmental*, vol. 227, pp. 114–122, 2018.

g-c3n4 under simulated sunlight irradiation: kinetics, mechanism, and antibacterial activity elimination," *Applied Catalysis B: Environmental*, vol. 227, pp. 114–122, 2018.

[74] W. Ben, B. Zhu, X. Yuan, Y. Zhang, M. Yang, and Z. Qiang, "Occurrence, removal and risk of organic micropollutants in wastewater treatment plants across china: Comparison of wastewater treatment processes," *Water research*, vol. 130, pp. 38–46, 2018.

[75] A. Suárez-Escobar, V. Rodríguez-González, C. Gallardo-Vega, E. Sarria, and L. Clavijo, "Ketoprofen degradation by surface reactive species on tio2, agxoy/moxoy/catalysts," *Materials Letters*, vol. 294, p. 129687, 2021.

[76] S. Ebrahimzadeh, B. Wols, A. Azzellino, B. J. Martijn, and J. P. van der Hoek, "Quantification and modelling of organic micropollutant removal by reverse osmosis (ro) drinking water treatment," *Journal of Water Process Engineering*, vol. 42, p. 102164, 2021.

[77] B. Maryam, V. Buscio, S. U. Odabasi, and H. Buyukgungor, "A study on behavior, interaction and rejection of paracetamol, diclofenac and ibuprofen (phacs) from wastewater by nanofiltration membranes," *Environmental Technology & Innovation*, vol. 18, p. 100641, 2020.

[78] B. Xu, F. Wu, X. Zhao, and H. Liao, "Benzotriazole removal from water by zn–al–o binary metal oxide adsorbent: Behavior, kinetics and mechanism," *Journal of Hazardous Materials*, vol. 184, no. 1-3, pp. 147–155, 2010.

[79] M. A. Décima, S. Marzeddu, M. Barchiesi, C. Di Marcantonio, A. Chiavola, and M. R. Boni, "A review on the removal of carbamazepine from aqueous solution by using activated carbon and biochar," *Sustainability*, vol. 13, no. 21, p. 11760, 2021.

[80] O. M. Couto Jr, I. Matos, I. M. da Fonseca, P. A. Arroyo, E. A. da Silva, and M. A. S. D. de Barros, "Effect of solution ph and influence of water hardness on caffeine adsorption onto activated carbons," *The Canadian Journal of Chemical Engineering*, vol. 93, no. 1, pp. 68–77, 2015.

[81] E. S. Massima Mouele, J. O. Tijani, M. Masikini, O. O. Fatoba, C. P. Eze, C. T. Onwordi, M. T. Zar Myint, H. H. Kyaw, J. Al-Sabahi, M. Al-Abri, *et al.*, "Spectroscopic measurements of dissolved o3, h2o2 and oh radicals in double cylindrical dielectric barrier discharge

technology: treatment of methylene blue dye simulated wastewater," *Plasma*, vol. 3, no. 2, pp. 59–91, 2020.

[82] B. Wols and C. Hofman-Caris, "Review of photochemical reaction constants of organic micropollutants required for uv advanced oxidation processes in water," *Water research*, vol. 46, no. 9, pp. 2815–2827, 2012.

[83] F. Li, Y. Kang, M. Chen, G. Liu, W. Lv, K. Yao, P. Chen, and H. Huang, "Photocatalytic degradation and removal mechanism of ibuprofen via monoclinic bivo4 under simulated solar light," *Chemosphere*, vol. 150, pp. 139–144, 2016.

[84] F. J. Real, F. J. Benitez, J. L. Acero, J. J. Sagasti, and F. Casas, "Kinetics of the chemical oxidation of the pharmaceuticals primidone, ketoprofen, and diatrizoate in ultrapure and natural waters," *Industrial & Engineering Chemistry Research*, vol. 48, no. 7, pp. 3380–3388, 2009.

[85] A. Alighardashi, R. S. Aghta, and H. Ebrahimzadeh, "Improvement of carbamazepine degradation by a three-dimensional electrochemical (3-ec) process," *International Journal of Environmental Research*, vol. 12, no. 4, pp. 451–458, 2018.

[86] M. Jiménez-Salcedo, M. Monge, and M. T. Tena, "The photocatalytic degradation of sodium diclofenac in different water matrices using g-c3n4 nanosheets: A study of the intermediate by-products and mechanism," *Journal of Environmental Chemical Engineering*, vol. 9, no. 5, p. 105827, 2021.

[87] C. B. Anucha, I. Altin, E. Bacaksiz, V. N. Stathopoulos, I. Polat, A. Yasar, and Ö. F. Yüksel, "Silver doped zinc stannate (ag-znsno3) for the photocatalytic degradation of caffeine under uv irradiation," *Water*, vol. 13, no. 9, p. 1290, 2021.

Appendix A

Degradation and kinetics data

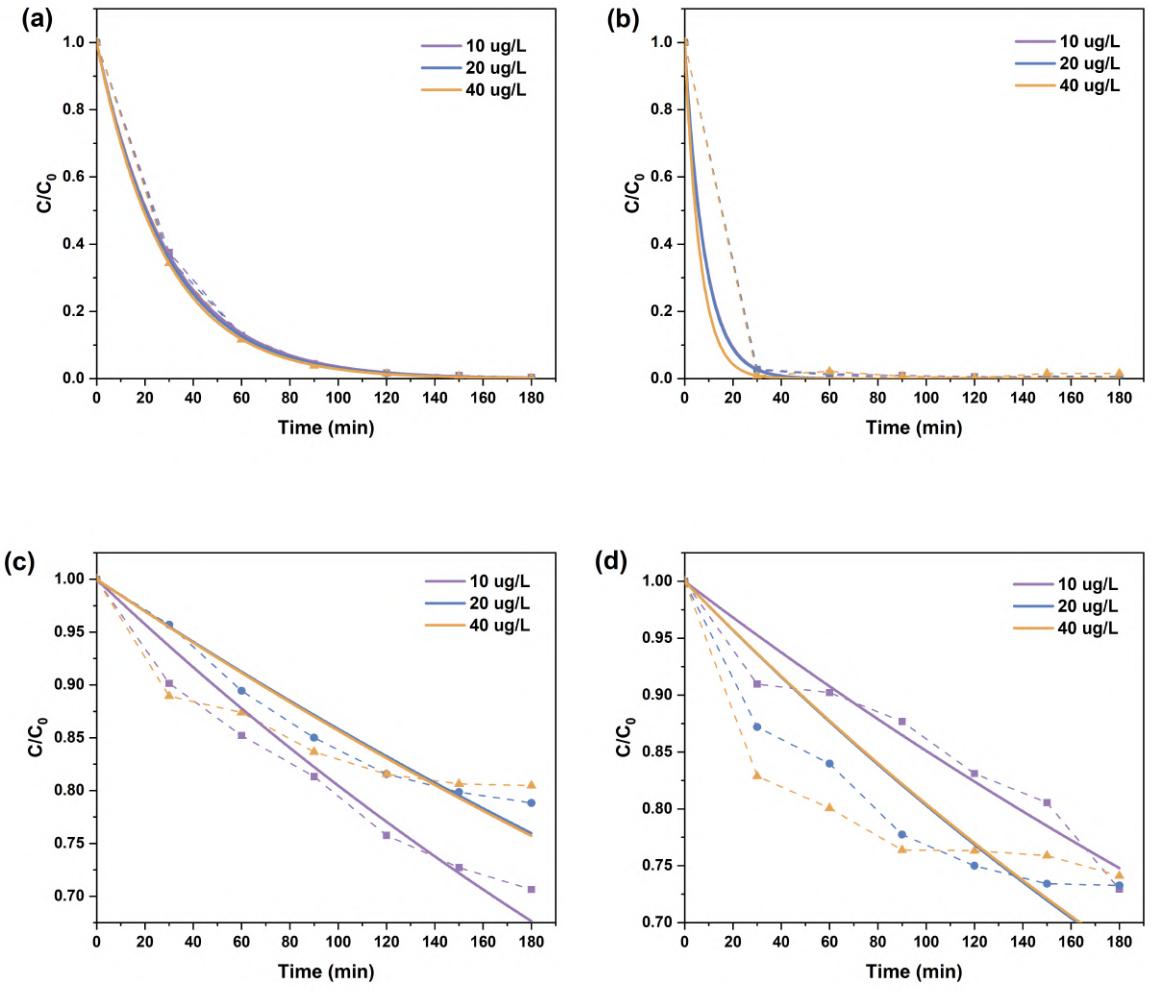

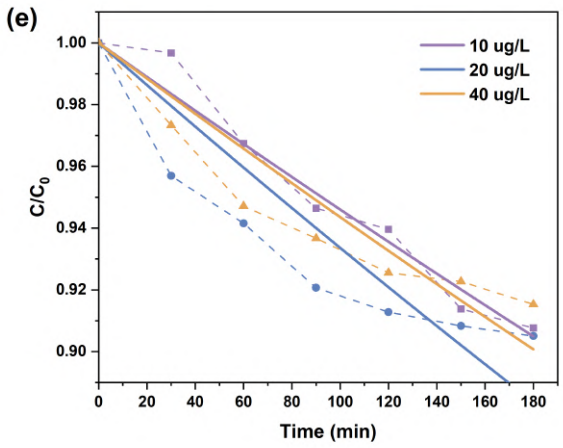

Figure A.1: Kinetics plots for the degradation experiments at initial concentration of 10, 20 and 40 $\mu g{\cdot}L^{-1}$ for (a) DIC, (b) KET, (c) BTA, (d) CBZ and (e) CAF.

Table A.1: Degradation efficiency and kinetics parameters of the five target OMPs by $BiVO_4/(TiO_2/GO)_{mix}$ photoanodes at initial concentration of 10, 20 and 40 $\mu g{\cdot}L^{-1}$.

OMPs	**Degradation efficiency (%)**	**k** (min^{-1})	$\mathbf{R^2}$
DIC (10 $\mu g{\cdot}L^{-1}$)	99.5880	0.0333	0.9998
DIC (20 $\mu g{\cdot}L^{-1}$)	99.8316	0.0344	0.9999
DIC (40 $\mu g{\cdot}L^{-1}$)	99.8280	0.0357	0.9999
KET (10 $\mu g{\cdot}L^{-1}$)	99.7820	0.1185	0.9996
KET (20 $\mu g{\cdot}L^{-1}$)	99.3758	0.1211	0.9997
KET (40 $\mu g{\cdot}L^{-1}$)	98.4462	0.1571	0.9988
BTA (10 $\mu g{\cdot}L^{-1}$)	29.3560	0.0022	0.9527
BTA (20 $\mu g{\cdot}L^{-1}$)	21.1742	0.0015	0.9524
BTA (40 $\mu g{\cdot}L^{-1}$)	19.5263	0.0016	0.6747
CBZ (10 $\mu g{\cdot}L^{-1}$)	27.0624	0.0016	0.9366
CBZ (20 $\mu g{\cdot}L^{-1}$)	26.7238	0.0022	0.7995
CBZ (40 $\mu g{\cdot}L^{-1}$)	25.8861	0.0022	0.4459
CAF (10 $\mu g{\cdot}L^{-1}$)	9.2346	5.5490E-4	0.9678
CAF (20 $\mu g{\cdot}L^{-1}$)	9.4924	6.8692E-4	0.7480
CAF (40 $\mu g{\cdot}L^{-1}$)	8.4718	5.8092E-4	0.8430

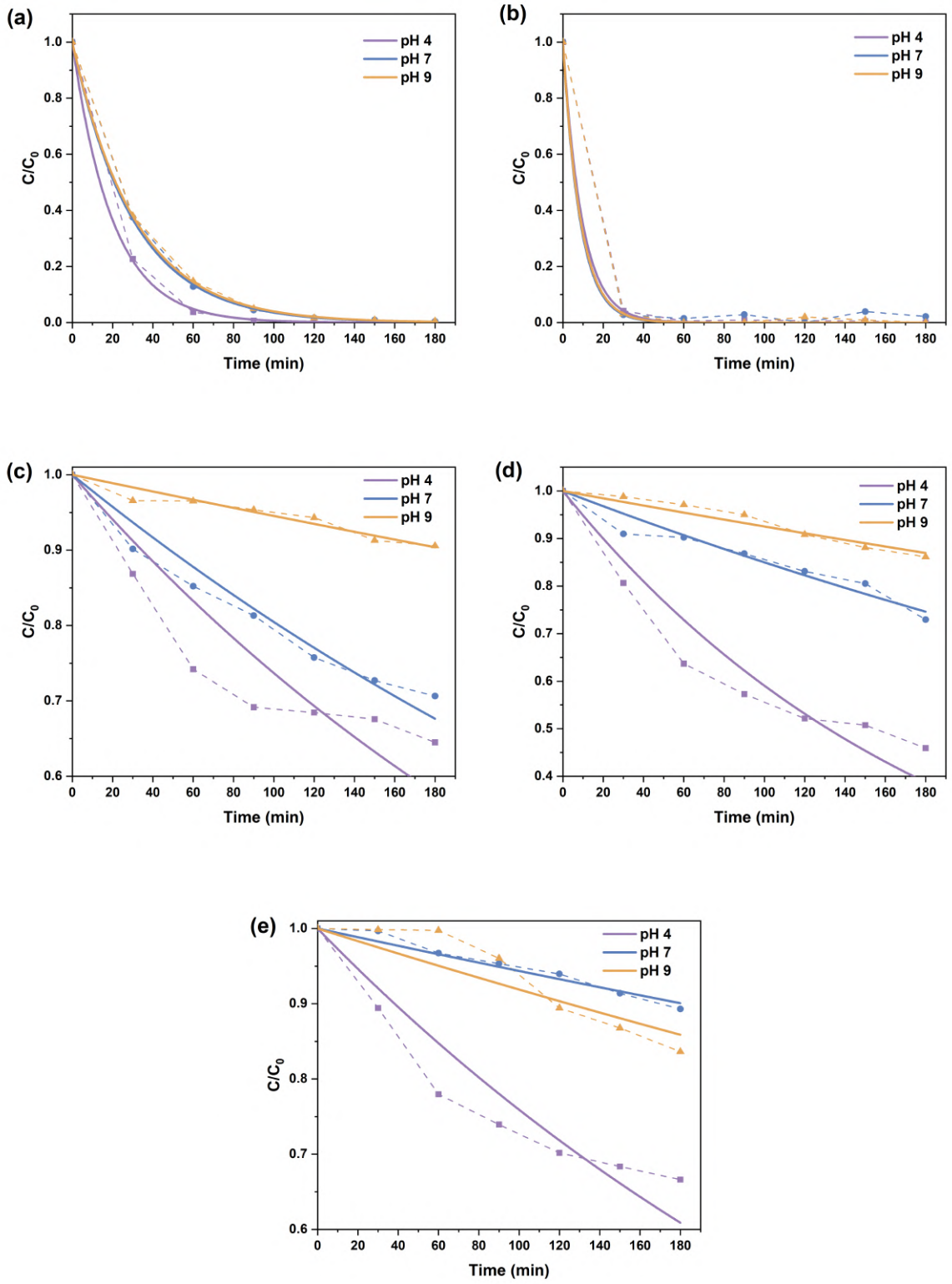

Figure A.2: Kinetics plots for the degradation experiments with initial pH of 3.5-4.0, 6.5-7.0 and 8.5-9.0 for (a) DIC, (b) KET, (c) BTA, (d) CBZ and (e) CAF.

Table A.2: Degradation efficiency and kinetics parameters of the five target OMPs by $BiVO_4/(TiO_2/GO)_{mix}$ photoanodes with initial pH of 3.5-4.0, 6.5-7.0 and 8.5-9.0.

OMPs	**Degradation efficiency (%)**	**k** (min^{-1})	$\mathbf{R^2}$
DIC (pH4)	99.9133	0.0503	0.9998
DIC (pH7)	99.5880	0.0333	0.9998
DIC (pH9)	99.5100	0.0322	0.9999
KET (pH4)	100.0000	0.1052	0.9998
KET (pH7)	97.8200	0.1184	0.9963
KET (pH9)	100.0000	0.1151	0.9994
BTA (pH4)	35.5025	0.0031	0.7878
BTA (pH7)	29.3561	0.0022	0.9527
BTA (pH9)	9.4316	5.6170E-4	0.9323
CBZ (pH4)	54.0737	0.0053	0.9057
CBZ (pH7)	27.0624	0.0016	0.9395
CBZ (pH9)	13.8498	7.7585E-4	0.9505
CAF (pH4)	33.3712	0.0028	0.8792
CAF (pH7)	10.6977	5.8075E-4	0.9656
CAF (pH9)	16.3644	8.4607E-4	0.83812

Table A.3: Degradation efficiency and kinetics parameters of the five target OMPs by $BiVO_4/(TiO_2/GO)_{mix}$ photoanodes after three cycles.

OMPs	**Degradation efficiency (%)**	**k** (min^{-1})	$\mathbf{R^2}$
DIC (Run1)	99.9133	0.0503	0.9998
DIC (Run2)	99.5653	0.03462	0.9999
DIC (Run3)	91.8728	0.0182	0.9072
BTA (Run1)	35.5025	0.0031	0.7878
BTA (Run2)	32.7250	0.0022	0.9527
BTA (Run3)	28.2266	5.6170E-4	0.9323
CBZ (Run1)	54.0737	0.0053	0.9057
CBZ (Run2)	47.6329	0.0041	0.9669
CBZ (Run3)	37.6015	0.0030	0.9754
CAF (Run1)	33.3712	0.0028	0.8792
CAF (Run2)	24.0186	0.0018	0.8896
CAF (Run3)	21.2837	0.0016	0.7152

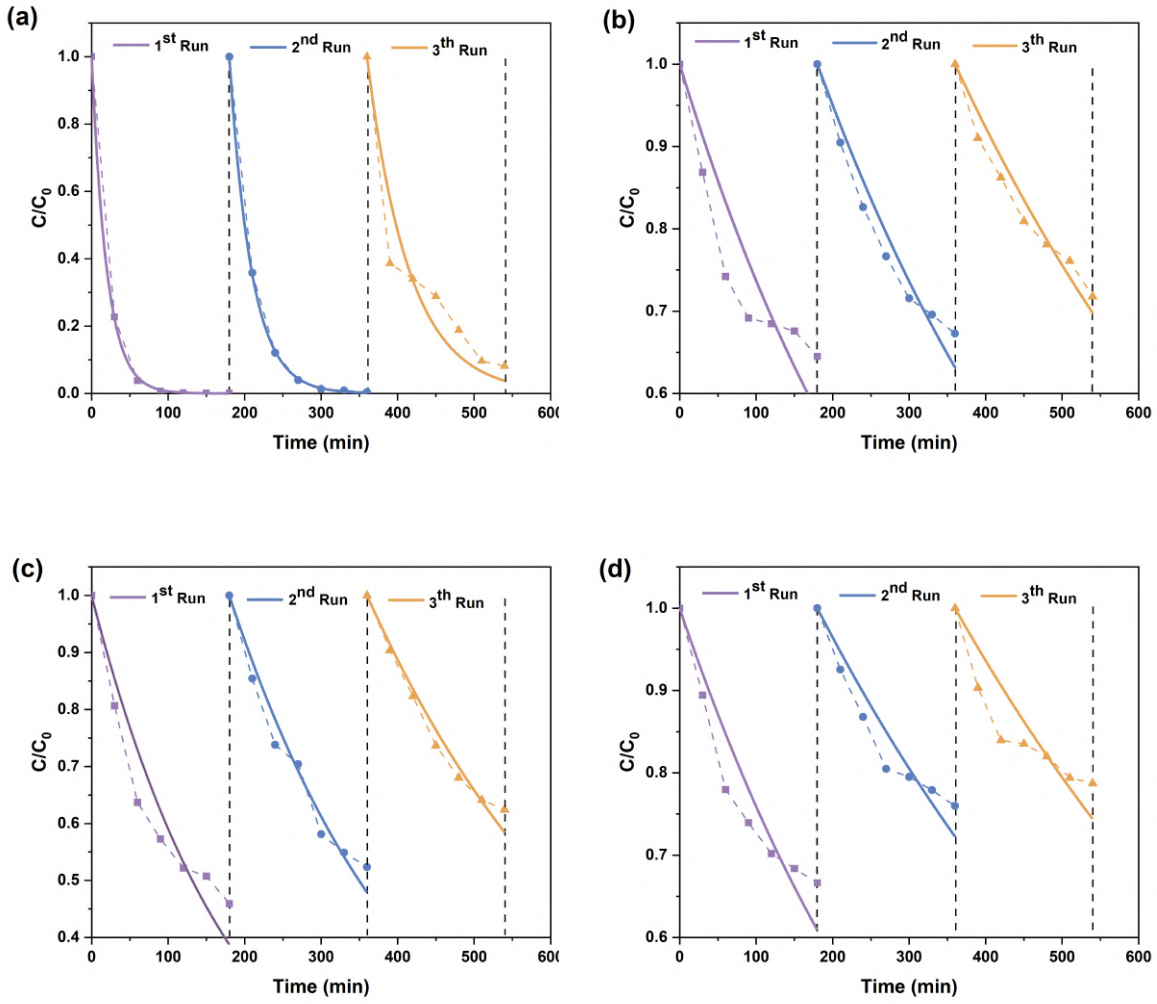

Figure A.3: Kinetics plots for the three-cycle degradation experiments for (a) DIC, (b) BTA, (c) CBZ and (d) CAF.